

เมทัลลอร์แกนิกเฟรมเวิร์ก เอ็มไอเอฟ-ไฟว์ สำหรับเป็นวัสดุเก็บแก๊สคาร์บอนไดออกไซด์
ศึกษาด้วยวิธีทางเคมีคอมพิวเตอร์

นายธนาวุฒิ พลอยมีรัมย์

วิทยานิพนธ์นี้เป็นส่วนหนึ่งของการศึกษาตามหลักสูตรปริญญาวิทยาศาสตรมหาบัณฑิต

สาขาวิชาปิโตรเคมีและวิทยาศาสตร์พอลิเมอร์

คณะวิทยาศาสตร์ จุฬาลงกรณ์มหาวิทยาลัย

ปีการศึกษา 2551

ลิขสิทธิ์ของจุฬาลงกรณ์มหาวิทยาลัย

**METAL ORGANIC FRAMEWORKS MOF-5 AS CARBON DIOXIDE
STORAGE STUDIED BY COMPUTATIONAL CHEMISTRY METHOD**

Mr. Tanawut Ploymeerusmee

A Thesis Submitted in Partial Fulfillment of the Requirements
for the Degree of Master of Science Program in Petrochemistry and Polymer Science
Faculty of Science
Chulalongkorn University
Academic Year 2008
Copyright of Chulalongkorn University

Thesis Title METAL ORGANIC FRAMEWORKS MOF-5 AS CARBON
DIOXIDE STORAGE STUDIED BY COMPUTATIONAL
CHEMISTRY METHOD
By Mr. Tanawut Ploymeerusmee
Field of Study Petrochemistry and Polymer Science
Thesis Advisor Professor Supot Hannongbua, Dr.rer.nat.
Thesis Co-Advisor Duangamol Nuntasri, Ph.D.

Accepted by the Faculty of Science, Chulalongkorn University in Partial
Fulfillment of the Requirements for the Master's Degree

..... Dean of the Faculty of Science
(Professor Supot Hannongbua, Dr.rer.nat.)

THESIS COMMITTEE

..... Chairman
(Assistant Professor Warinthorn Chavasiri, Ph.D.)

..... Thesis Advisor
(Professor Supot Hannongbua, Dr.rer.nat.)

..... Thesis Co-Advisor
(Duangamol Nuntasri, Ph.D.)

..... Examiner
(Assistant Professor Somsak Pianwanit, Ph.D.)

..... External Examiner
(Arthorn Loisuangsinn, Ph.D.)

ธนาวุฒิ พลอยมีร์คีมี : เมทัลออร์แกนิกเฟรมเวิร์ก เอ็มโอเอฟ-ไฟฟ์ สำหรับเป็นวัสดุเก็บ
แก๊สคาร์บอนไดออกไซด์ศึกษาด้วยวิธีทางเคมีคอมพิวเตอร์. (METAL ORGANIC
FRAMEWORKS MOF-5 AS CARBON DIOXIDE STORAGE STUDIED
BY COMPUTATIONAL CHEMISTRY METHOD) อ.ที่ปรึกษาวิทยานิพนธ์
หลัก: ศ.ดร. สุพจน์ หารหนองบัว, อ.ที่ปรึกษาวิทยานิพนธ์ร่วม: อ. ดร.ดวงกมล นันทศรี,
70 หน้า.

การปล่อยคาร์บอนไดออกไซด์ เช่นจากโรงงานอุตสาหกรรมและโรงงานผลิตกระแสไฟฟ้า
เป็นสาเหตุสำคัญของปรากฏการณ์โลกร้อน โครงร่างโลหะ-อินทรีย์ ได้ถูกใช้เป็นตัวหลักในการ
เก็บคาร์บอนไดออกไซด์ที่เกิดขึ้น โครงร่างโลหะ-อินทรีย์ ประกอบด้วย กลุ่มของซิงค์ออกไซด์ไอออน
เทต และส่วนเชื่อมต่อกันที่เป็นสารอะโรมาติกอินทรีย์ชนิดต่างๆ ทำให้ได้เป็นชุดของสารที่มีโครงร่าง
ตาข่ายของโครงร่างโลหะอินทรีย์ที่หลากหลาย โดยงานวิจัยนี้ได้ใช้ คลัสเตอร์ 3 ชนิด คือ
 $(Zn_4O)_2(COOCH_3)_{10}(COO)_2C_6H_4$, $(Zn_4O)_3(COOCH_3)_{14}(COO)_4(C_6H_4)_2$ และ
 $(Zn_4O)_4(COOCH_3)_{18}(COO)_6(C_6H_4)_3$ เป็นตัวแทน หลังจากนั้นจึงใช้วิธี ONIOM เบสิตเซต
MP2/6-31G(d,p) : HF/6-31G(d,p) ที่มีการแก้ไขโดย BSSE มาใช้ในการคำนวณเพื่อหา
บริเวณดูดซับของคาร์บอนไดออกไซด์ในโครงร่างโลหะ-อินทรีย์ ผลการคำนวณพบว่า คลัสเตอร์
 $(Zn_4O)_4(COOCH_3)_{18}(COO)_6(C_6H_4)_3$ มีขนาดเพียงพอสำหรับการอธิบายการดูดซับ
นอกจากนี้ยังพบว่าบริเวณมุมเป็นบริเวณที่เหมาะสมสำหรับการดูดซับคาร์บอนไดออกไซด์ ใน
ส่วนที่สองเป็นการคำนวณพลวัตเชิงโมเลกุลของโครงร่างโลหะ-อินทรีย์ขนาด $2 \times 2 \times 2$ ซึ่งบรรจุ
คาร์บอนไดออกไซด์จำนวน 8, 64, 128, 256 และ 512 โมเลกุลต่อกล่องลูกบาศก์จำลอง
(MPC) ที่อุณหภูมิ 300 เคลวิน ผลที่ได้สอดคล้องกับผลการคำนวณ ONIOM กล่าวคือ การดูดซับ
ของคาร์บอนไดออกไซด์เกิดได้ดีที่บริเวณมุมของ MOF-5 ผลที่น่าสนใจเกิดขึ้นที่การคำนวณที่
ความเข้มข้น 512MPC ซึ่งพบการจัดรูปแบบของคาร์บอนไดออกไซด์เป็นชั้นที่สองซึ่งเกิดการยึด
เหนี่ยวอย่างอ่อนๆ ที่บริเวณที่ว่างรอบมุมของ MOF-5 ทั้งนี้โดยมีตัวเลขโคออร์ดิเนชันเฉลี่ยของ
จำนวนคาร์บอนไดออกไซด์ที่บริเวณมุมและที่บริเวณตัวเชื่อมเท่ากับ 2.9 และ 3.1 โมเลกุล
ตามลำดับ

สาขาวิชาปิโตรเคมีและวิทยาศาสตร์พอลิเมอร์...ลายมือชื่อ.....
ปีการศึกษา.....2551.....ลายมือชื่อ อ.ที่ปรึกษาวิทยานิพนธ์หลัก.....
ลายมือชื่อ อ.ที่ปรึกษาวิทยานิพนธ์ร่วม.....

4972318423: PETROCHEMISTRY AND POLYMER SCIENCE

KEYWORDS: Metal Organic Frameworks / MOF-5 / ONIOM / Molecular Dynamic Simulation / Carbon Dioxide Storage.

TANAWUT POLYMEERUSMEE: METAL ORGANIC FRAMEWORKS MOF-5 AS CARBON DIOXIDE STORAGE STUDIED BY COMPUTATIONAL CHEMISTRY METHOD. THESIS ADVISOR: PROF. SUPOT HANNONGBUA, Dr.rer.nat., THESIS CO-ADVISOR: DUANGAMOL NUNTASRI, Ph.D., 70 pp.

The excess emission of carbon dioxide (CO₂), *e.g.*, releasing from manufactory and power plant generator, is the major cause of global warming. Metal-Organic Frameworks (MOFs) become a primary target for CO₂ storage production. MOFs consist of zinc oxo acetate clusters and various organic aromatic linkers providing a series of Isorecticular MOFs (IRMOFs). In this work, three model clusters, (Zn₄O)₂(COOCH₃)₁₀(COO)₂C₆H₄, (Zn₄O)₃(COOCH₃)₁₄(COO)₄(C₆H₄)₂ and (Zn₄O)₄(COOCH₃)₁₈(COO)₆(C₆H₄)₃ were used to represent the ligand, then, BSSE corrected ONIOM method (MP2/6-31G(d,p) : HF/6-31G(d,p)) were applied in order to determine the adsorption site of CO₂ in MOFs. The results indicate that the cluster (Zn₄O)₄(COOCH₃)₁₈(COO)₆(C₆H₄)₃ is sufficient to describe the adsorption and the MOF-5 corner is the preferential binding site of CO₂ molecule. In the second part, MD simulations of 2×2×2 lattice units of MOF-5 with the loading of 8, 64, 128, 256, 512 molecules of CO₂ per simulation cube (MPC) were performed at 300 K. The obtained results are in agreement with those found from ONIOM calculations that CO₂ prefers to absorb at the MOF-5 corner site. Interestingly, conclusion at MPC=512, the CO₂ was found to form second layer coordinated weakly to fill the rest space around the MOF-5 corner. The average coordination numbers of CO₂ at the corner and the linker sites are 2.9 and 3.1 molecules, respectively.

Field of Study: Petrochemistry and Polymer Science Student's Signature.....

Academic Year: 2008 Advisor's Signature.....

Co-Advisor's Signature.....

ACKNOWLEDGEMENTS

I would like to express my gratitude to all those who gave me the possibility to complete this thesis.

Firstly, I would like to thank my family for all their support. Especially, my mother and sister who care for me as same as care yourself. Furthermore, I am grateful thanks for a kindness of my supervisor Prof. Dr.rer.nat. Supot Hannongbua who never blames me in my mistake but he concerns and cheers me up as always. This thesis may not succeed if I never received too much assistance and suggestion form him. I give a great respect to the importance person, Aj Supot. One lady, who is indispensable person, is Dr. Oraphan Saengsawang. She teaches me in MD-simulation technique and gives me some suggestion for solving in many problems. Moreover, she works hard to help me complete this thesis, thank you so much Dr. Oraphan Sangsawang. Afterward, I would like to appreciate Asst. Prof. Dr. Tawun Remsungnen who gives me a suggestion in MD-simulation while I stayed in KonKhan University.

I would like to special thanks to Asst. Prof. Dr. Warinthorn Chavasiri, Asst. Prof. Dr. Somsak Pianwanit, Dr. Arthorn Loisruangsin, Dr. Duangamol Nuntasri who act as the thesis committee.

I thank all of my friends who walk together and cheer up me not only in the bad time but also in good time. For all CCUC members, I extend my glad to them for many help in works and lifestyles.

Finally, I would like to acknowledge National Center of Excellence for Petroleum, Petrochemicals, and Advanced Materials (NCE-PPAM) for financial supporting and the computational chemistry unit cell (CCUC) at Department of Chemistry, Faculty of Science, Chulalongkorn University where supports me in all facilities and computer resources.

CONTENTS

	Page
ABSTRACT IN THAI	iv
ABSTRACT IN ENGLISH	v
ACKNOWLEDGEMENTS	vi
CONTENTS	vii
LIST OF TABLES	x
LIST OF FIGURES	xi
LIST OF ABBREVIATIONS	xiii
CHAPTER I INTRODUCTION	1
1.1 Research Rationale	1
1.2 Carbon Dioxide Emission	1
1.3 Metal Organic Frameworks	2
1.4 A Series of Isoreticular Metal Organic Framewroks	3
1.5 Industrial Applications	4
1.5.1 Catalysis	4
1.5.2 Gas Separation	5
1.5.3 Gas Storage	5
1.6 Motivation Background	6
1.7 Scope of This Study	8
CHAPTER II THEORY BACKGROUND	9
2.1 Computational Quantum Mechanics	9
2.1.1 Quantum mechanics	9
2.1.2 Schrödinger equation	10
2.1.3 Born-Oppenheimer approximation	10
2.1.4 Hartree-Fock Approximation	11

2.1.5	Density Functional Theory.	11
2.1.6	Møller-Plesset Perturbation Theory.	12
2.1.7	Basis Set.	13
2.1.7.2	Single- ζ , Multiple- ζ , and Split-Valence.	13
2.1.7.2	Polarization Function.	14
2.1.7.3	Diffuse Function.	14
2.1.8	Basis Set Superposition Error.	15
2.1.9	The ONIOM Approach.	16
2.1.9.1	Hybrid Calculation with ONIOM.	17
2.2	Molecular Dynamic Simulations.	18
2.2.1	Introduction.	18
2.2.2	Molecular Interactions.	19
2.2.2.1	Non-bonded Interaction.	19
2.2.2.2	Bonding Potential.	20
2.3	Periodic Boundary Conditions.	21
2.4	Radial Distribution Function.	22
2.5	Cut-off.	23
CHAPTER III METHODOLOGY		24
3.1	Quantum Chemical Calculations	24
3.1.1	Initial Structure of MOF-5 Model.	24
3.1.2	The Model.	25
3.1.3	ONIOM Calculations Including BSSE.	26
3.2	Molecular Dynamic Simulations.	27
3.2.1	Initial Lattice Structure.	27
3.2.2	Force Field Parameters.	28
3.2.3	Molecular Dynamic Simulation Details.	29

CHAPTER IV RESULTS AND DISCUSSIONS.	30
4.1 Quantum Chemical Calculations.	30
4.1.1 Geometries of the MOF-5.	30
4.1.2 Effect of an Unbalance of the Basis Sets.	32
4.1.3 MOF-5 and CO ₂ Binding.	34
4.2 Molecular Dynamic Simulations.	36
4.2.1 Structure of CO ₂ at the MOF-5 Corner.	36
4.2.2 Structure of CO ₂ at the MOF-5 Linker.	38
4.2.3 Orientation of CO ₂ Around the MOF-5 Binding Site.	39
4.2.4 CO ₂ -CO ₂ Radial Distribution Functions.	41
CHAPTER V CONCLUSIONS.	43
REFERENCES.	45
APPENDICES	50
APPENDIX A: Publication.	51
APPENDIX B: Manuscript.	58
VITAE.	70

LIST OF TABLES

Table	Page
3.1	Potential parameters for non-bonded interaction in MOF-5. 28
4.1	Selected bond distances and bond angles obtained from the geometry optimizations for the two clusters shown in Figure 3.1 where the experimental data [6] and the other theoretical calculations [50,51] were also given for comparison (see Figure 3.1 for atomic labels).. 31
4.2	ONIOM binding energies with BSSE corrections and the corresponding distances between Cg point of MOF-5 in the three cluster models (SINGLE, DOUBLE and TRIPLE in figure 3.2a) and CO ₂ in two orientations (and ⊥) in which the distance was measured from Cg of linker to C atom of CO ₂ 35
4.3	ONIOM binding energies with BSSE corrections and the corresponding distances between Cg point of MOF-5 in the three cluster models (SINGLE, DOUBLE and TRIPLE in figure 3.2a) and CO ₂ in two orientations (and ⊥) in which the distance was measured from O1 of corner to C atom of CO ₂ 36

LIST OF FIGURES

Figure		Page
1.1	Unit cell of MOF-5 or IRMOF-1.	3
1.2	A series of isorecticular metal organic frameworks.	3
1.3	Various derivative of carboxylate group.	4
1.4	MOF-177 framework.	6
2.1	The two and three layered ONIOM extrapolation scheme.	17
2.2	The Lennard-Jones potential.	20
2.3	Periodic boundary conditions. The central box is outlined by a thicker line.	22
2.4	Radial distribution functions use a spherical shell of thickness δr	23
3.1	(a) A single fragment of MOF-5 consisting of two corners and one linker and (b) the whole MOF-5 unit cell which were generated as initial structure to be used in this study where C _g donates center of ass of the benzene ring.	24
3.2	Representation of the calculation models where rectangular and filled-circle represent linker and corner, respectively, and dot-circle denotes the model part for which high level of accuracy in the ONIOM calculation was applied. (a) Models SINGLE, DOUBLE and TRIPLE represent the MOF fragments containing one, two and three units as oriented, where one unit of the model is compose of two corners connected by a linker (Figure 1a). Orientation of CO ₂ molecule binds in parallel and perpendicular to the linker (b1) and corner (b2) binding sites.	26
3.3	The 2×2×2 unit cells of MOF-5 lattice structure used in the simulation.	27
4.1	ONIOM binding energies with and without BSSE corrections for CO ₂ /MOF-5 in parallel () configuration for all systems. For the linker and corner calculations, the distances were measured from the C atom of CO ₂ to C _g and O1, respectively.	32

4.2	ONIOM binding energies with and without BSSE corrections for CO ₂ /MOF-5 in perpendicular (\perp) configuration for all systems. For the linker and corner calculations, the distances were measured from the C atom of CO ₂ to Cg and O1, respectively.	33
4.3	(a)-(b) Radial distribution functions (RDF) for the 5 loadings of CO ₂ , centered at O1 of MOF-5 (see Figure 1 for atomic labels) to O and C atoms of CO ₂ , respectively. (c) Distribution of the corresponding coordination number calculated up to the first minimum of 4.90 Å of the O1-O RDF where the average coordination numbers (\overline{CN}) were also shown.	38
4.4	(a)-(b) Radial distribution functions (RDF) for the 5 loadings of CO ₂ , centered at the middle of benzene ring of the MOF-5 linker, Cg (see text for definition), to O and C atoms of CO ₂ , respectively. (c) Distribution of the corresponding coordination number averaged up to the first minimum of 6.00 Å of the Cg-O RDF where the average coordination numbers (\overline{CN}) were also shown.	39
4.5	Distribution of the angles θ and ϕ representing orientation of CO ₂ lying under the first peak of the O1-O RDF (a) and the Cg-O RDF (b) where the plots for the 2 peaks of the O1-C RDF at the loading of 512 MPC was given separately (b) (see text for more details).	41
4.6	(a)-(b) C-C and C-O Radial distribution functions (RDF) for the 5 loadings of CO ₂ . (c) Distribution of the corresponding coordination number averaged up to the first minimum of 5.50 Å of the C-C RDF where the average coordination numbers (\overline{CN}) were also shown. . . .	42

LIST OF ABBREVIATIONS

B3LYP	=	Beck's three parameter hybrid functional using the LYP correlation function
BDC	=	Benzene dicarboxylate
BSSE	=	Basis set superposition error
BTB	=	1,3,5-benzenetribenzoate
CN	=	Coordination number
CP	=	Counterpoise method
DFT	=	Density functional theory
HF	=	Hartree-Fock
IMOMM	=	Integrated molecular orbital and molecular mechanics
IMOMO	=	Integrated molecular orbital and molecular orbital method
IRMOFs	=	Isoreticular metal organic frameworks
KS	=	Kohn-Sham
LCAO	=	Linear combination of atomic orbitals
LYP	=	Lee-Yang-Parr functional
MO	=	Molecular orbital
MOFs	=	Metal organic frameworks
MP2	=	Møller-Plesset perturbation theory second order.
MPC	=	Molecular per simulation cubic
ONIOM	=	Our own n-layered integrated molecular orbital and molecular mechanics
RDF	=	Radial distribution function
SBU _s	=	Secondary building units
STO	=	Slater type orbital
STO-3G	=	Slater type orbital approximated by 3 gaussian type orbitals

CHAPTER I

INTRODUCTION

1.1 Research Rationale

Natural fuel such as coal, petroleum oils and natural gases are mainly used by human in many activities, *e.g.*, transportation, industry and electric power station. These lead activities not only gain desired products, heat, energy and electricity, but also undesired ones, greenhouse gas such as carbon dioxide (CO₂) *etc.* Amount of CO₂ released to atmosphere causes serious environment problem, consequently, global warming. Gas storage application is initiated and continuously developed to reduce amount of undesired gas like CO₂ in atmosphere. The materials which have high surface areas and stability are required to construct the best storage.

As promising candidates to fulfill these requirements, the metal organic frameworks (MOFs) have attracted attention of scientists because of their unique properties, *i.e.*, very well defined structure as well as high surface area and stability under 300 K. Moreover, their structure is able to be modified in order to provide the larger volume in gas storage application. The basic understanding of gas behavior inside MOF such as the adsorption site and preferential gas orientation is one of the key factors to improve and develop gas storage technology. The obtained basic information is expected to be the guideline for designation of the new material with high capability in gas storage application.

1.2 Carbon Dioxide Emission

Since Industrial revolution in 18th century, energy resources such as coal, petroleum oil and natural gas were used as fuel in manufactory and burned in power plant to produce electricity. Due to those activities, the amount of carbon dioxide released into the atmosphere has been rising extensively during last 150 years. The major cause of global warming is the emission of green house gasses like carbon dioxide, methane, *etc.* into the atmosphere. The large amount of carbon dioxide emission plays the important role in global warming. The reduction of CO₂ emission

have been initiated and developed. Options for decreasing greenhouse gas emission include reducing energy consumption, increasing energy efficiency and use, adopting lower or zero carbon fuels and reducing greenhouse gas from non-energy sources. A further option for reducing carbon dioxide emission from energy production is capture and storage, permitting the production of carbon dioxide but preventing its emission. Until now, many materials were attended to study in carbon dioxide storage, *e.g.*, carbonnanotube [1], zeolite [2-3] and metal organic frameworks [4-5]. The amount of carbon dioxide uptake depends on surface area of each material. In this study, metal organic framework was applied because it has a high surface area and pore volume.

1.3 Metal Organic Frameworks

Metal organic frameworks (MOFs) are a new class of nanoporous materials which become a promising material for gas storage, gas separation and catalysis applications. In 1999, Omar Yaghi and co-worker were firstly discovered a novel material called MOF-5 with high surface area approximately at $2900 \text{ m}^2/\text{g}$ as shown in Figure 1.1 [6]. The unit cell of MOFs is consisted of zinc oxide cluster (pink circle) linked with dicarboxylate group (blue circle) in three-dimensional cubic framework providing a crystalline structure. It is a strong bond providing a high robust framework with well-defined structure. For example, resulting in a MOF-5 structure was demonstrated that it has higher surface area and pore volume than most porous crystalline material. The first target of this material was used in hydrogen storage application for increase in hydrogen storage capacity [7]. Both linker and oxide cluster can be modified by synthesis with different organic linkage and metal oxide, respectively. In my thesis, MOF-5 was interested because it is a prototype of MOFs with the simple secondary building unit (SBU) providing sufficient MOFs material for binding energy calculation.

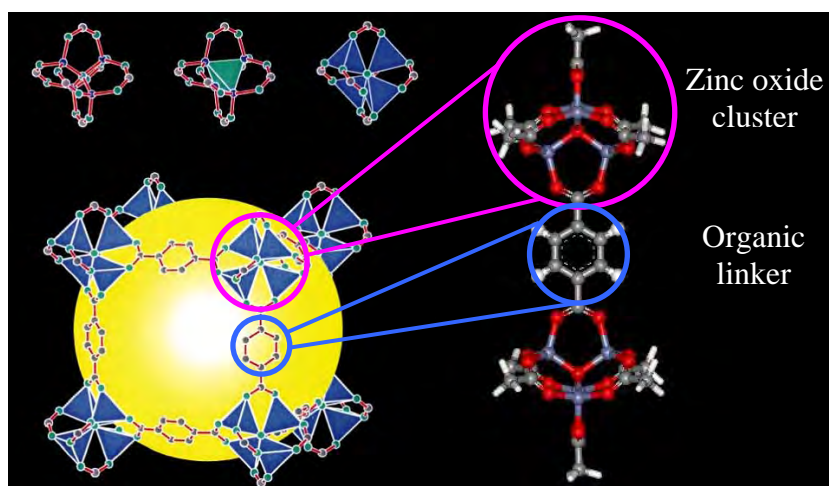


Figure 1.1 Unit cell of MOF-5 or IRMOF-1.

1.4 A Series of Isoreticular Metal Organic Frameworks

A large series of isoreticular metal organic frameworks (IRMOFs) [8-9] has been produced in which each member shares the same cubic topology adopted by the prototype MOF-5 as shown in Figure 1.2. Cluster size and surface area of these materials depend on organic linker which made from various derivative of carboxylate group as shown in Figure 1.3. When carboxylate group was more steric hindrance, surface area was decreased, for instance, IRMOF-1 to IRMOF-7. The pore expansion was founded in case of long linkage molecule.

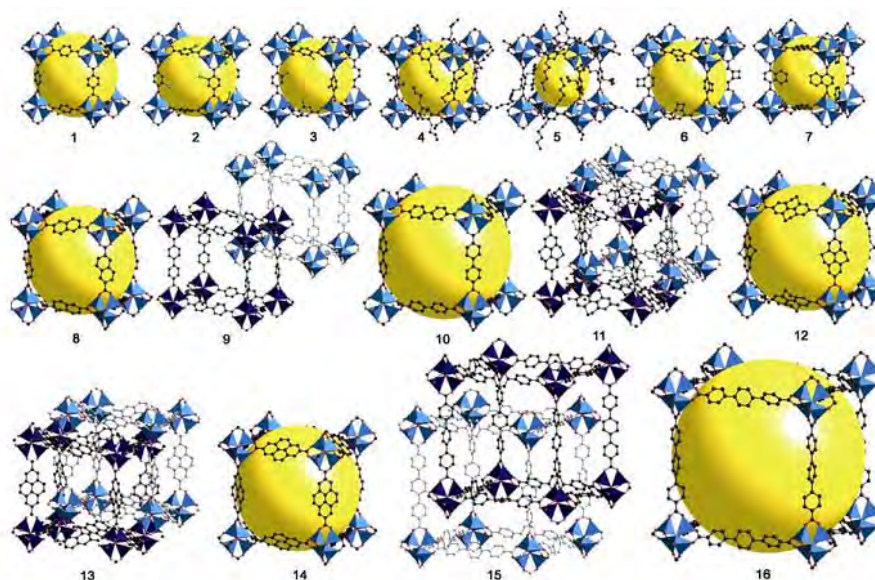


Figure 1.2 A series of isoreticular metal organic frameworks.

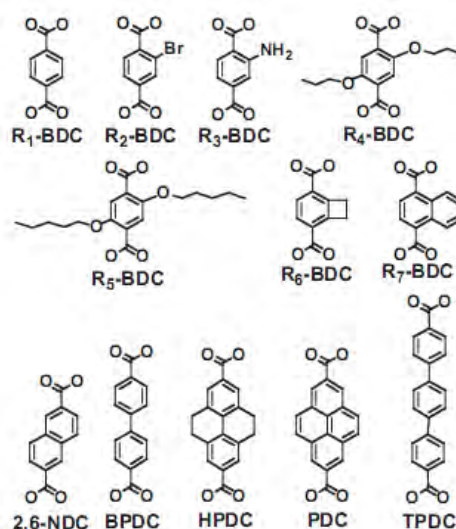


Figure.1.3 Various derivative of carboxylate group.

1.5 Industrial Applications

More than 100 kinds of metal organic framework has been synthesized [10] with high surface area, it becomes a promising material applied in various field of industry applications.

1.5.1 Catalysis

Generally, catalysts can be classified into two groups; the homogeneous and heterogeneous one. Homogeneous catalysts are ones which are in the same phase as the reactants while heterogeneous catalysts are ones which are in a different phase. In industrial applications, heterogeneous catalysts are often preferred over homogeneous catalysts. One reason for that is product/catalyst can be easier to separate after the process. The porous material becomes a promising target as catalyst in petrochemical industry because it has a high surface area. The common material, zeolite [11], was used as heterogeneous catalyst in olefin polymerization industrial. The invention related to a porous heterogeneous catalyst material leads to interesting in a metal organic frameworks [12]. One of its application is hydrocarbon transformation. In framework, inorganic cornerstones connected by organic bridges, characterized in that as organic bridges are used ligands having a complexed catalytically active metal. The metals are preferably palladium and platinum. The ligands preferably contain nitrogen

donor groups for complexing the catalytically active metal and carboxylate groups connecting to the inorganic cornerstones.

One member of IRMOFs series, IRMOF-3, consists of amino group in linker, which shows basic catalyst in Knoevenagel condensation of benzaldehyde with two methylene active compounds of different pK_a , viz. ethyl cyanoacetate ($pK_a \leq 9$) and ethyl acetoacetate ($pK_a \leq 10.7$) [13].

1.5.2 Gas Separation

Membrane technology is economically competitive with alternative separation technologies such as distillation, crystallization, absorption, or solvent extraction for many chemical separations. Gas mixtures can be effectively separated by synthetic membranes. The performance of MOF-5 membrane separation was investigated in various mixture gases. In every case, mixture effects play a crucial role in determining the membrane performance [14]. In separation of alkanes with gas chromatography, MOF-508 was selected to packing in column. The result can be described that alkane can be separated with this method [15]. The Cu-MOF was used in removal of sulfur odorant components from natural gas. When compare with Norit-carbon, Cu-MOF is a powerful material for the separation of polar components from non-polar gases [16].

1.5.3 Gas Storage

Generally, metal organic frame works is high surface area, which is appropriate for gas storage application. The world record of the highest surface area of MOF is MOF-177 with unprecedented surface area about $4,500 \text{ m}^2/\text{g}$. MOF-177 unit cell was fabricated by triangular 1,3,5-benzenetribenzoate (BTB) units connecting with octahedral zinc(II) carboxylate clusters, $\text{Zn}_4\text{O}(\text{CO}_2)_6$, such that each zinc cluster is attached to six BTB units. The applications were used in hydrogen [17] and carbon dioxide storage [4]. Remarkably in carbon dioxide storage, at 35 bar, a container filled with MOF-177 can uptake 9 times the amount of carbon dioxide in a container without adsorbent. The MOF-177 framework is shown in Figure 1.4. The application of hydrogen storage was applied in hydrogen fuel cell or hydrogen car tank fields. Moreover, the new type MOFs was fabricated with high surface area concept providing more capacity in light gas storage.

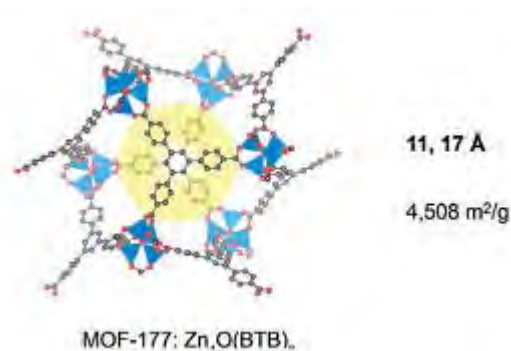


Figure 1.4 MOF-177 framework.

1.6 Motivation Background

It was further step of innovation in material science when Omar M. Yaghi and co-workers discovered a novel material, so called, metal organic frameworks which have a high surface area and large pore volume. With their distinguish properties, MOFs were studied by many scientists, mostly in gas storage application, both experimental and theoretical fields.

In 2001, after MOF was discovered, Jaheon Kim *et al.* [18] illustrated MOFs applicability to rationalizing MOF crystal structures by analysis of nine new MOFs with SBU of MOFs structure. The result indicated that SBU approach provides new and simplifying principles to classify the complex structures. Symmetrical and simple SBUs such as tetrahedra in MOF-31 and -32 and squares and tetrahedral in MOF-35 are easier to prediction, and they lead to predictable geometry of whole structures.

In 2003, Tina Düren *et al.* [19] investigated in the adsorption characteristics of novel metal-organic materials and compare them with the characteristics of two zeolites, MCM-41, and different carbon nanotubes for CH₄ by using molecular simulation. The factors of influencing methane adsorption are depend upon the surface area, the capacity or free volume, the strength of the energetic interaction, and the pore size distribution.

In 2003, Nathaniel L. Rosi *et al.* [7] indicated the binding site of hydrogen storage in MOF-5 by neutron scattering spectroscopy of the rotational transitions. The hydrogen binding sites are located at corner and linker unit of MOF-5 with 4.5 weight percent of hydrogen loading at 78 K.

In 2005, Claudia F. Braga and Ricardo L. Longo [20] calculated molecular structure of the IRMOFs based on Zn₄O(RCOO)₆, R = CH₃ and Ph, and

$(\text{CH}_3\text{COO})_5(\text{Zn}_4\text{O})(\text{OOC}-\text{C}_6\text{H}_3\text{X}-\text{COO})_6(\text{Zn}_4\text{O})(\text{CH}_3\text{COO})_5$, X = H, Br and NH_2 , with AM1, PM3, HF/6-31G, HF/6-31G**, B3LYP/6-31G, B3LYP/6-31G** and ONIOM(HF/6-31G:PM3) methods. The AM1 and PM3 methods seem appropriate for a (semi-) quantitative description of the molecular structures of the IRMOFs based on $\text{Zn}_4\text{O}(\text{RCOO})_6$ SBUs. Ab initio (HF) and hybrid DFT (B3LYP) yielded good agree with experimental results. The ONIOM(HF/6-31G:PM3) or higher method seem to be choice for describing the molecular structure and the interaction of molecule(s) with the walls of the IRMOF's cavity.

In 2005, Qingyuan Yang and Chongli Zhong [21] performed a molecular simulation study on the adsorption and diffusion of hydrogen in MOFs to describe in details of the underlying mechanisms. The result shows that metal oxide clusters are preferential adsorption sites for hydrogen in MOFs and the effect of the organic linkers becomes apparent with increasing pressure.

In 2006, Sanyue Wang *et al.* [22] studied on adsorption separation of $\text{CO}_2/\text{CH}_4/\text{C}_2\text{H}_6$ mixtures in a manganese formate metal organic framework (Mn-MOF) compare with other materials. The pore size plays the important role in adsorption separation of CO_2 -alkane mixtures. Mn-MOF provides the most appropriate pore size, leading to the largest selectivity for these mixtures, especially, in ternary mixture. It's promising material for gas separation in petrochemical industry.

In 2006, Qingyuan Yang and Chongli Zhong [23] used MOF-5 and Cu-BTC for purification of synthetic gas with molecular simulation. This work shows that both the geometry and pore size affect the separation characteristics of MOFs largely. The Cu-BTC is better in separation efficiency than MOF-5.

In 2007, Jonathan L. Belof *et al.* [24] modeled hydrogen sorption in MOF. The simulations demonstrate that hydrogen interacts with the MOF via three principle attractive potential energy contributions: Van der Waals, charge-quadrupole, and induction. Indeed, polarization interactions in the MOF lead to two distinct populations of dipolar hydrogen that are identified from the simulations that should be experimentally discernible using, for example, Raman spectroscopy. Since polarization interactions are significantly enhanced by the presence of a charged framework with narrow pore, MOFs are excellent hydrogen storage candidates.

In 2008, Qingyuan Yang *et al.* [25] investigated the effects of organic linker, pore size and topology, and the electrostatic fields on the adsorption and diffusion

behaviors of CO₂ in nine types of MOFs. Comparison with other material, MOFs have the highest CO₂ adsorption capacity and the suitable pore size is between 1.0 and 2.0 nm. Although the CO₂-MOF electrostatic interaction can contribute as large as 30% to the total adsorption capacity at low pressures, it decreases monotonically with increasing pressure and contributes only a few percent at high pressures.

In 2008, Jeffery A. Greathouse and Mark D. Allendorf [26] designed to validate the flexible force field for IRMOF-1 compare with rigid force field. The simulations were also carried out with adsorbed guests, including ethanol, cyclohexane, and several chloromethanes. A rigid force field with slight modified is much poorer agreement with experimental data. Additionally, a flexible force field approach is required when simulating framework stability because of physical changes or the presence of adsorbates.

Previous studies were interest in efficiency of each MOFs in term of qualitative and quantitative without describing in structure property of guest molecule in pore of MOFs. Then in this study was pay attention to understand the structure property of guest molecule in MOFs by using computational method.

1.7 Scope of This Study

The investigation of behavior of CO₂ in absorbate MOF-5 can be classified into two of computational calculations.

Firstly, quantum calculation, because of whole unit cell of MOF-5 was not calculated with high accuracy method, and then MOF-5 was modified in 3 models. To seeking adequate model of CO₂/MOF-5 binding, ONIOM method was approached with BSSE correction. The binding site of CO₂ and optimal orientation into MOF-5 were examined as well.

Secondly, the behavior of CO₂ in MOF-5 was examined by using molecular dynamic simulation. The number of CO₂ loading, *i.e.*, 8, 64, 128, 256 and 512 molecules per simulation cube were determined at 300 K, for instant, radial distribution function was used to describe structure property of these systems.

CHAPTER II

THEORY BACKGROUND

The theoretical chemistry may be defined as a mathematical description of chemistry, whereas computational chemistry is usually used when a mathematical method is sufficiently well developed that it can be automated for implementation on a computer. Note that the words exact and perfect do not appear here, as very few aspects of chemistry can be computed exactly. However, almost every aspect of chemistry can be described in a qualitative or approximate quantitative computational scheme.

2.1 Computational Quantum Mechanics

2.1.1 Quantum Mechanics

Classical mechanics [27, 28] is inadequate form describing systems composed of small particles such as electrons, atoms and molecules. Therefore the missing from classical mechanics is the description of wavelike properties of matter that predominates with small particles. Quantum mechanics takes into account the wavelike properties of matter when solving mechanical problems.

The word quantum comes from Latin (quantus, “how much?”, plural quanta) and was first used in our sense by Max Planck in 1900, as an adjective and noun, to denote the constrained quantities or amounts in which energy can be emitted or absorbed. Although the term quantum mechanics was apparently first used by Born (of the Born–Oppenheimer approximation, section 2.1.3) in 1924, in contrast to classical mechanics, the matrix algebra and differential equation techniques that we now associate with the term were presented in 1925 and 1926. The mathematics and laws of quantum mechanics that must be used to explain wavelike properties cause a dramatic change in the way mechanical problems must be solved. In quantum mechanics, the mathematics that yields physically measurable properties is obtained from mathematical operations with an indirect physical correlation.

Molecules are made of nuclei and electrons, and quantum chemistry deals, fundamentally, with the motion of electrons under the influence of the electromagnetic force exerted by nuclear charges. An understanding of the behavior of electrons in molecules, and thus of the structures and reactions of molecules, rests on quantum mechanics and in particular on that adornment of quantum chemistry, the Schrödinger equation.

2.1.2 Schrödinger Equation

Quantum mechanics describe molecules in terms of interactions among nuclei and electrons, and molecular geometry in terms of minimum energy arrangements of nuclei. All quantum mechanical methods ultimately trace back to the Schrödinger equation [29-31], which for the special case of hydrogen atom may be solved exactly. Solutions to Schrödinger's equation describe not only atomic and subatomic systems, electrons and atoms, but also macroscopic systems, possibly even the whole universe. Schrödinger's equation can be mathematically transformed into Heisenberg's matrix mechanics, and into Feynman's path integral formulation. The Schrödinger equation describes time in a way that is inconvenient for relativistic theories, a problem which is not as severe in Heisenberg's formulation and completely absent in the path integral.

The total energy for this kind of system has five contributions: kinetic energies of each nuclei and electron (T_e and T_n), attraction between each electron and nuclei (V_{en}), internuclear and interelectronic repulsion potential energy (V_{ee} and V_{nn}).

The many-electron Schrödinger equation cannot be solved exactly (or at least has not been solved) even for a simple two-electron system such as helium atom or hydrogen molecule. Approximations need to be introduced to provide practical methods.

2.1.3 Born-Oppenheimer approximation

The Born-Oppenheimer approximation is central to quantum chemistry. In many-particle molecular systems, accurate wave functions for such systems are extremely difficult to express because of the correlated motions of particles. Under typically physical conditions, the nuclei of molecular systems are moving much more

slower than the electrons. Due to the great difference in motion between the nuclei and the electrons, the electrons are capable of instantaneously adjusting to any change in position of the nuclei. The Born-Oppenheimer approximation is the assumption that the electronic motion and the nuclear motion in molecules can be separated. It leads to a molecular wave function in terms of electron positions and nuclear positions.

Hence, one way to simplify the Schrödinger equation for molecular systems is to assume that the nuclei do not move. It means that the electron motion is determined for a fixed position of the nuclei making the constant distances between nuclei-nuclei. It implies that the nuclear kinetic energy term is taken to be independent of the electrons, correlation in the attractive electron-nuclear potential energy term is eliminated and the repulsive nuclear-nuclear potential energy term becomes a simply evaluated constant for a given geometry. This is called the Born-Oppenheimer approximation [27, 30].

2.1.4 Hartree-Fock Approximation

Finding and describing approximate solution to the electronic Schrödinger equation has been a major preoccupation of quantum chemists since the birth of quantum mechanics. Except for the very simplest cases like one-electron problem, quantum chemists are faced with many-electron problems. Individual electrons are confined to functions termed molecular orbitals, each of which is determined by assuming that the electron is moving within an average field of all the other electrons. The simplest antisymmetric wave function is written in the form of a single determinant (a so-called Slater determinant), which can be used to describe the ground state of an N -electron system. The essential of the Hartree-Fock approximation [32] is to replace the complicated many-electron problem by a one-electron problem in which electron-electron repulsion is treated in an average way. The procedure for solving the Hartree-Fock equation is called the self-consistent-field (SCF) method.

2.1.5 Density Functional Theory

One approach to the treatment of electron correlation is referred to as density functional theory. The Density Functional Theory (DFT) is a computationally efficient way of including electron correlation [33]. The system is described by an

electron density, rather than a sum of independent electrons, and the Hamiltonian is then only dependent on position and atomic number of the nuclei and the total number of electrons. The governing equation is still the electronic Schrödinger equation but the total energy of the system is expressed as a function of the electron density.

DFT is an exact theory and the only approximation in term of exchange correlation energy is unknown. The basis sets for these Kohn-Sham (KS)-orbitals have fewer requirements than those in Hartree-Fock. They are not needed for calculating exchange and Coulomb interaction which are the most work consuming part of the Hartree-Fock method. This, and the fact that DFT account for electron correlation, make DFT very useful for larger systems. However, the crucial task in DFT is to find an accurate exchange correlation functional. The most popular exchange-correlation functional is the B3LYP functional [34, 35]. It consists of several functionals, including the HF exact exchange energy in a three-parametric scheme.

2.1.6 Møller-Plesset Perturbation Theory

Møller-Plesset perturbation theory [36, 37] is a tool of perturbation theory, which provides a method for adding excitations to the Hartree-Fock wave function and therefore including the effect of electron correlation. A perturbation theory is developed for treating a system of n electrons in which the Hartree-Fock solution appears as the zero-order approximation. It is shown by this development that the first order correction for the energy and the charge density of the system is zero. The expression for the second-order correction for the energy greatly simplifies because of the special property of the zero-order solution. This level of theory is referred to as MP2. To obtain an improvement on the HF energy it is therefore necessary to use Møller-Plesset perturbation theory at least second order. It is pointed out that the development of the higher approximation involves only calculations based on a definite one-body problem.

Systematic studies of MP perturbation theory have shown that it is not necessarily a convergent theory at high orders. The convergence properties can be slow, rapid, oscillatory, regular, highly erratic or simply non-existent, depending on the precise chemical system or basis set.

2.1.7 Basis Set

The set of mathematical functions that constructs the molecular orbital (MO) in the linear combination of atomic orbitals (LCAO) is called a basis set, which is expanded as a linear combination of such functions with weights or coefficients to be determined. Usually these functions are atomic orbitals, in that they are centered on atoms, but functions centered in bonds or lone pairs, and pairs of functions centered in the two lobes of a p orbital, have been used. Additionally, basis sets composed of sets of plane waves down to a cutoff wavelength are often used, especially in calculations involving systems with periodic boundary conditions [30, 38].

2.1.7.1 Single- ζ , Multiple- ζ , and Split-Valence

The STO-3G basis set is what is known as a “single- ζ ” basis set, or, more commonly, a “minimal” basis set. This nomenclature implies that there is one and only one basis function defined for each type of orbital core through valence. Thus for H and He, there is only a 1s function. For Li to Ne, there are five functions, 1s, 2s, 2p_x, 2p_y, and 2p_z. For Na to Ar, 3s, 3p_x, 3p_y, 3p_z are added to the second-row set, making a total of nine functions, etc. Because the minimal basis set is so small, it is so small, it is not recommended for consistent and accurate predictions of molecular energies. However, their simple structure provides a good tool for visualizing qualitative aspects of chemical bonding.

One way to increase the flexibility of a basis set is to “decontract” it. That is, we might imagine taking the STO-3G basis set, and instead of constructing each basis function as a sum of three Gaussians, we could construct two basis functions for each AO, the first being a contraction of the first two primitive Gaussians, while the second would simply be the normalized third primitive. This prescription would not double the size of our basis set, since we would have all the same individual integrals to evaluate as previously, but the size of our secular equation would be increased. A basis set with two functions for each AO is called a “double- ζ ” basis. Of course, we could decontract further, and treat each primitive as a full-fledged basis function, in which case we would have a “triple- ζ ” basis, and we could then decide to add more functions indefinitely creating higher and higher multiple- ζ basis sets.

The reason for this is that core orbitals are only weakly affected by chemical bonding. Valence orbitals, on the other hand, can vary widely as a function of

chemical bonding. Atoms bonded to significantly more electronegative elements take on partial positive charge from loss of valence electrons, and thus their remaining density is distributed more compactly. The reverse is true when the bonding is a more electropositive element. From a chemical standpoint, then, there is more to be gained by having flexibility in the valence basis functions than in the core, and recognition of this phenomenon led to the development of so-called “split-valence” or “valence-multiple- ζ ” basis sets. The core orbitals are represented by minimal basis set whereas the valence shell orbitals are represented by more than one basis function such as 3-21G, 6-21G, 4-31G, 6-31G, and 6-31G, which have one contracted that is a linear combination of three primitive Gaussian for each inner-shell atomic orbital and two basis function, one contracted Gaussian function that is a linear combination of two primitive Gaussian function, for each valence orbital. If there is valence-triple- ζ , like 6-311G, use there sizes of contracted functions for each orbital-type.

2.1.7.2 Polarization Function

Polarized basis sets allow some small contributions from the unfilled orbital, which is required for the ground state for atomic description by adding orbitals with angular momentum beyond. Pople and co-workers introduced a simple nomenclature scheme to indicate the presence of these functions, the “*” (star). Thus, 6-31G* implies a set of d functions added to polarize the p functions in 6-31G. A second star ** implies p functions on H and He, e.g., 6-31G**. To use more than one set of polarization functions in modern calculation, the standard nomenclature for the Pople basis sets now typically includes an explicit enumeration of those functions instead of the star nomenclature.

2.1.7.3 Diffuse Function

When a basis set does not have the flexibility necessary to allow a weakly bound electron to localize far from the remaining density (such as molecular with lone pairs, anions and other systems with significant negative charge, systems in their excited states, and system with low ionization potentials), significant errors in energies and other molecular properties can occur. In the Pople family of basis sets, the presence of diffuse function is indicated by a “+” in the basis set name. The 6-

31+G(d) indicates that heavy atoms have been augmented with an additional one s and one set of p functions having small exponents.

2.1.8 Basis Set Superposition Error

Suppose we wish to calculate the energy of formation of a bimolecular complex, such as the energy of formation of a hydrogen-bond water dimer. [39] Such complexes are sometimes referred to as “supermolecule”. One might expect that this energy value could be obtained by first calculating the energy of a single water molecule, then calculating the energy of the dimer, and finally subtracting the energy of the two isolated water molecules (the reactant) from that of the dimer (the product). However, the energy difference obtained by such an approach will invariably be an overestimate of the true value. The discrepancy arises from a phenomenon known as *basis set superposition error* (BSSE). As the two water molecules approach each other, the energy of the system falls not only because of the favorable intermolecular interactions but also because the basis function on each molecule provide a better description of the electronic structure around the other molecule. It is clear that the BSSE would be expected to be particularly significant when small, inadequate basis sets are used which do not provide for an adequate representation of the electron distribution far from the nuclei, particularly in the region where non-covalent interactions are strongest. One way to estimate the basis set superposition error is via the counterpoise correction method of Boys and Bernardi, in which the entire basis set is included in all calculations. Interaction energies between two atoms or molecules A and B are typically calculated as the energy difference between the product complex AB and its components A and B as followed.



$$\Delta E = E(AB) - [E(A) + E(B)] \quad [2.2]$$

The calculation of the energy of the individual species A is performed in the presence of “ghost” orbitals of B ; that is, without the nuclei or electrons of B . A similar calculation is performed for B using ghost orbitals on A . An alternative approach is to use a basis in which the orbital exponents and contraction coefficients have been optimized for molecular calculations rather than for atoms. The relevance of the basis

set superposition error and its dependence upon the basis set and the level of theory employed.

2.1.9 The ONIOM Approach

The standard ab initio molecular orbital (MO) approach, especially one including electron correlation to the highest level, is well-known to be computationally expensive. The high dependency of the computation time on the number of atoms in the molecule makes it impossible to study most chemical systems at this level of theory. Furthermore, in theoretical studies of larger systems, it's impossible to calculate the whole system with high theory level as well.

To solve their problems, the ONIOM [40-42] (our own n-layered integrated molecular orbital and molecular mechanics) approach has been proposed and shown to be successful in reproducing benchmark calculations and experimental results. It's an onion skin-like extrapolation method which is developed by Morokuma and co-workers that enables different levels of theory to be applied to different parts of a molecule in system and combined to produce a consistent energy expression. According to Morokuma and co-workers proposed the Integrated Molecular Orbital and Molecular Mechanics (IMOMM) method, the system is partitioned into 2 parts. Afterwards, it was realized that the extrapolation scheme in a combined MO + MO method, which was referred to as the Integrated Molecular Orbital and Molecular Orbital Method (IMOMO). Subsequently, the integration of more than two methods was succeeded, and the whole series of integrated methods was named the ONIOM method. Hence, IMOMO encompasses both two-layered ONIOM2 (MO:MO) and three-layered ONIOM3 (MO:MO:MO) and IMOMM is in principle equivalent to ONIOM2 (MO:MM) and ONIOM3 (MO:MO:MM). Thus, interesting or difficult part of the system is treated with more accurate method while he remains of the system are treated with the less accurate method. By this approach, a lot computational time can be saved. Finally, the main idea of this method is to perform a high-level calculation on just a small part of the system and to include the effects of the remainder at lower levels of theory, with the end result being of similar accuracy to a high-level calculation on the full system.

2.1.9.1 Hybrid Calculation with ONIOM

In the two-layered ONIOM method requires a high and low level of theory and a real and model molecular geometry. The energy at the high-level of theory for the real geometry is estimated as

$$E_{(High,Real)} = E_{(Low,Real)} + [E_{(High,Model)} - E_{(Low,Model)}] \quad [2.3]$$

Using the terminology of Morokuma et al., the full molecular geometry including all atoms is referred to as the real geometry and it is treated using a low-level of theory. A subset of these atoms, referred to as the model geometry, is treated using both the low-level and a high-level of theory. A three-layer model also introduces intermediate model geometry and a medium level of theory. The concept of the ONIOM method is represented schematically in Figure 2.1. For instance, ONIOM2, beginning at $E_{(Low,Model)}$, the extrapolation to the high-level calculation ($E_{(High,Model)} - E_{(Low,Model)}$) and the extrapolation to the real system ($E_{(Low,Real)} - E_{(Low,Model)}$) are assumed to produce an estimate for $E_{(High,Real)}$.

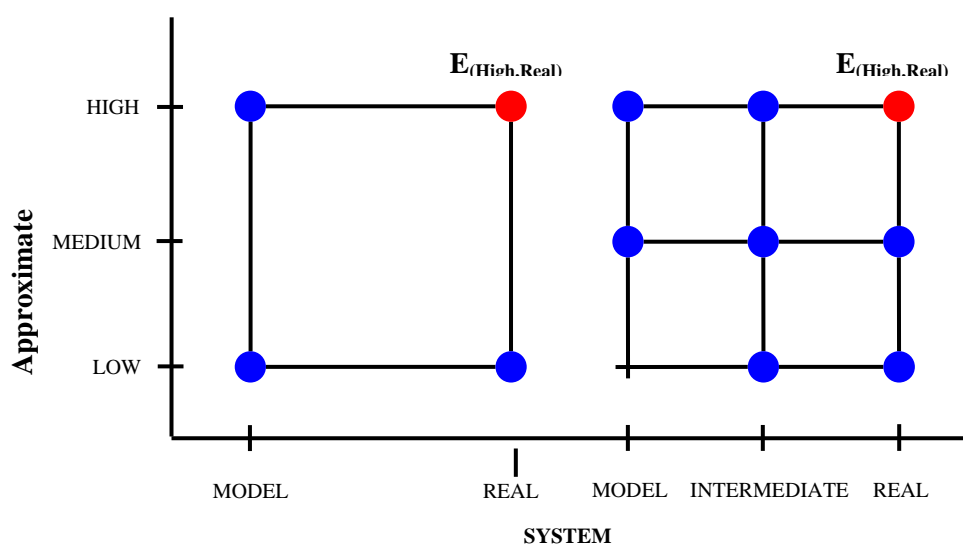


Figure 2.1 The two and three layered ONIOM extrapolation scheme.

As same as ONIOM2, $E_{(High,Real)}$ for ONIOM3 was procedured.

2.2 Molecular Dynamic Simulations

2.2.1 Introduction

Molecular dynamics [43] is a simulation of the time-dependent behavior of a molecular system, such as vibrational motion or Brownian motion. It requires a way to compute the energy of the system, most often using a molecular mechanics calculation. This energy expression is used to compute the forces on the atoms for any given geometry. The steps in a molecular dynamics simulation of an equilibrium system are as follows:

1. Choose initial positions for the atoms. For a molecule, this is whatever geometry is available, not necessarily an optimized geometry.
2. Choose an initial set of atom velocities. These are usually chosen to obey a Boltzmann distribution for some temperature, then normalized so that the net momentum for the entire system is zero (it is not a flowing system).
3. Compute the momentum of each atom from its velocity and mass.
4. Compute the forces on each atom from the energy expression. This is usually a molecular mechanics force field designed to be used in dynamical simulations.
5. Compute new positions for the atoms a short time later, called the time step. This is a numerical integration of Newton's equations of motion using the information obtained in the previous steps.
6. Compute new velocities and accelerations for the atoms.
7. Repeat steps 3 through 6.
8. Repeat this iteration long enough for the system to reach equilibrium. In this case, equilibrium is not the lowest energy configuration; it is a configuration that is reasonable for the system with the given amount of energy.

9. Once the system has reached equilibrium, begin saving the atomic coordinates every few iterations. This information is typically saved every 5 to 25 iterations. This list of coordinates over time is called a trajectory.

10. Continue iterating and saving data until enough data have been collected to give results with the desired accuracy.

11. Analyze the trajectories to obtain information about the system. This might be determined by computing radial distribution functions, diffusion coefficients, vibrational motions, or any other property computable from this information.

2.2.2 Molecular Interactions

2.2.2.1 Non-bonded Interaction

The non-bonded energy represents the pair-wise sum of the energies of all possible interacting non-bonded atoms. The non-bonded terms are usually considered in two groups, one comprising van der Waals attractions and the other electrostatic interactions [44].

Electrostatic Interactions

Each element can attract electrons differently, giving rise to an unequal distribution of charge in a molecule. This charge distribution can be represented in a number of ways, one common approach being an arrangement of fractional point charges throughout the molecule. These charges are designed to reproduce the electrostatic properties of the molecule. If the charges are restricted to the nuclear centers they are often referred to as partial atomic charges or net atomic charges. The electrostatic interaction between two molecules (or between different parts of the same molecule) is then calculated as a sum of interactions between pairs of point charges, using Coulomb's law.

Van Der Waals Interactions

Electrostatic interactions cannot account for all of the non-bonded interactions in a system. The rare gas atoms are an obvious example; all of the multipole moments of a rare gas atom are zero and so there can be no dipole-dipole or dipole-induced dipole interactions. But there clearly must be interactions between the atoms, how else could rare gases have liquid and solid phases or show deviations from ideal gas behavior? Deviations from ideal gas behavior were famously quantitated by van der Waals, thus the forces that give rise to such deviations are often referred to as van der Waals forces. The van der Waals attraction occurs at short range, and rapidly dies off as the interacting atoms move apart by a few Angstroms. Repulsion occurs when the distance between interacting atoms becomes even slightly less than the sum of their contact radii. Repulsion is modeled by an equation that is designed to rapidly blow up at close distances. The energy term that describes attraction/repulsion provides for a smooth transition between these two regimes. These effects are often modeled using a Lennard-Jones equation, as shown in the following plot: where i and j were represented as atom i and j .

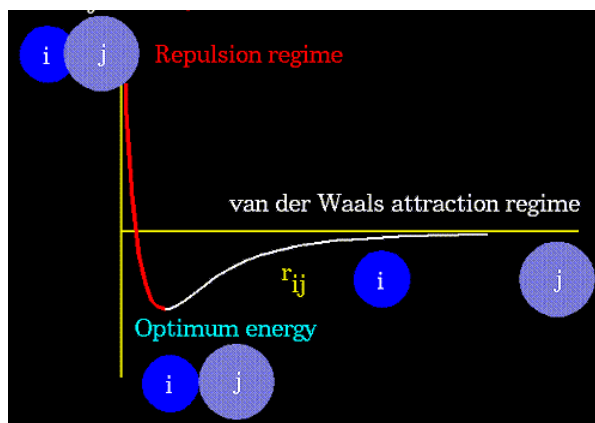


Figure 2.2 The Lennard-Jones potential.

2.2.2.2 Bonding Potential

Consider covalent bond atom, energy of molecule is described in terms of a sum of contributions arising from three distortions from ideal bond distances, bond angles and torsion angles [28, 38]. Firstly, bond energy is a function for stretching a

bond between two atoms which is most simply given in term of quadratic Hook's law form. The second, the energy required for bending angle formed by three atoms, where this is a bond between A and B, and between B and C, is a basic function in term of Hook's law as well as bonding term. Finally, the energy change associated with rotation around B-C bond in a four atom sequence A-B-C-D, where A-B, B-C and C-D are bonded, which represent is a function of combination of sine and cosine functions.

2.3 Periodic Boundary Conditions

The computer simulation programs were applied to predict and study the properties of a system in bulk. In the real system, we are not interested in surface effects. But our simulations track only a small number of particles in order not to slow down the computation. As a result, most molecules are near the edge of the sample that is near its surface. Therefore, it looks like we cannot avoid surface effects in our computations. The system size would have to be extremely large to ensure that the surface has only a small influence on the bulk properties, but this system would be too large to simulate.

Surface effects can be ignored for all computational system sizes if we use *periodic boundary conditions* [44]. In periodic boundary conditions, the cubical simulation box is replicated throughout space to form an infinite lattice. In the course of the simulation, when a molecule moves in the central box, its periodic image in every one of the other boxes moves with exactly the same orientation in exactly the same way. Thus, as a molecule leaves the central box, one of its images will enter through the opposite face. There are no walls at the boundary of the central box, and the system has no surface. The central box simply forms a convenient coordinate system for measuring locations of the N molecules. For example, a two-dimensional of periodic system is shown in Figure 2.. As a particle moves through a boundary, all its corresponding images move across their corresponding boundaries. The number of particles in the central box (and hence in the entire system) is conserved.

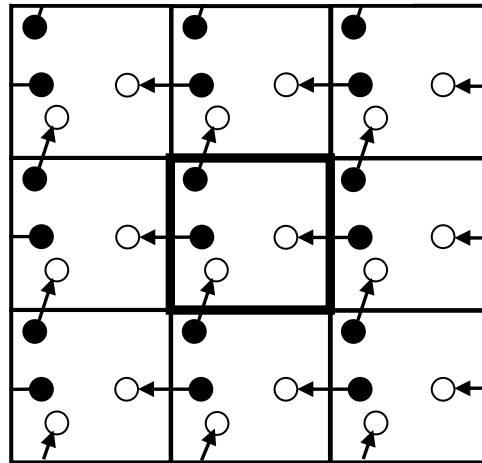


Figure 2.3 Periodic boundary conditions. The central box is outlined by a thicker line.

2.4 Radial Distribution Function

Radial distribution function (RDF) [44] is one of statistic mechanic that describes how the density of surrounding matter varies as a function of the distance from a particular point. Suppose, for example, when there are two solutes dissolved in water, the Brownian motion separates them by different distances r at different times. The RDF gives the probability of finding a particle in the distance r from another particle which is a useful tool to describe the structure of a system, particularly of liquids. In experimental, RDF can be measured using X-ray diffraction which is compared with the results obtained from the simulation. The basic RDF is the ratio between average density at distance from any determined atom r and the overall number density. The evaluation of RDF was represented in $g(r)$ which shows in Equation 2.4.

$$g(r) = \frac{N(r)}{\rho \Delta V(r)} \quad [2.4]$$

where $\Delta V(r)$ is a volume of spherical shell of thickness δr at distance r from a chosen atom. ρ is a number of particles per unit volume. A number of particles in the volume $\Delta V(r)$ are collected as $N(r)$.

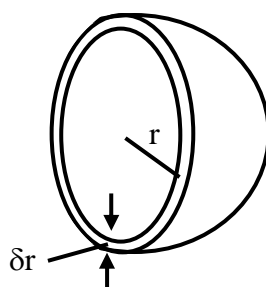


Figure 2.4 Radial distribution functions use a spherical shell of thickness δr .

2.5 Cut-off [38]

In the limit of large molecules, the computational time for calculating the force field energy grows approximately as the square of the number of atoms. The majority of these non-bonded energy contributions are numerically very small, as distance of atom pair is large. A considerable saving in computer time can be achieved by truncating the van der Waals potential at some distance. If the distance is larger than this cutoff, the contribution is neglected which avoids the calculation of distances between all pair of atoms. The introduction of a cut-off distance, beyond which E_{vdw} is set to zero, is quite reasonable as the neglected contributions are small. This is not true for the other part of the non-bonded energy, the Coulomb interaction. Contrary to the van der Waals energy, which falls off as R^{-6} , the charge-charge interaction varies as R^{-1} . This is actually true only for the interaction between molecules carrying a net charge. The charge distribution in neutral molecules or fragments makes the long-range interaction behave as a dipole-dipole interaction.

In this study, quantum chemical calculation and molecular dynamic simulation were performed with Gaussian 03 [46] and DL POLY 2 [47] packages, respectively.

CHAPTER III

METHODOLOGY

In this chapter, the optimal structure of MOF-5 lattice and preferential adsorption site of CO₂ in MOF-5 were investigated using quantum chemical calculations. In addition, the adsorption behavior of CO₂ in MOF-5 at different loading was examined by molecular dynamic simulations.

3.1 Quantum Chemical Calculations

3.1.1 Initial Structure of MOF-5 model

A column consisting of two corners connected by a linker, $(Zn_4O)_2(COOCH_3)_{10}(COO)_2C_6H_4$, was generated (Figure 3.1a). It was, then, used to build up the whole MOF-5 unit cell (Figure 3.1b). Aimed to get reliable geometries of the MOF-5 relative to experimental data [5], the two fragments (Figure 3.1a and 3.1b) were fully optimized using various quantum mechanical methods (semi-empirical, HF and DFT) and basis sets. All optimization and energy calculation were performed using Gaussian03 [45].

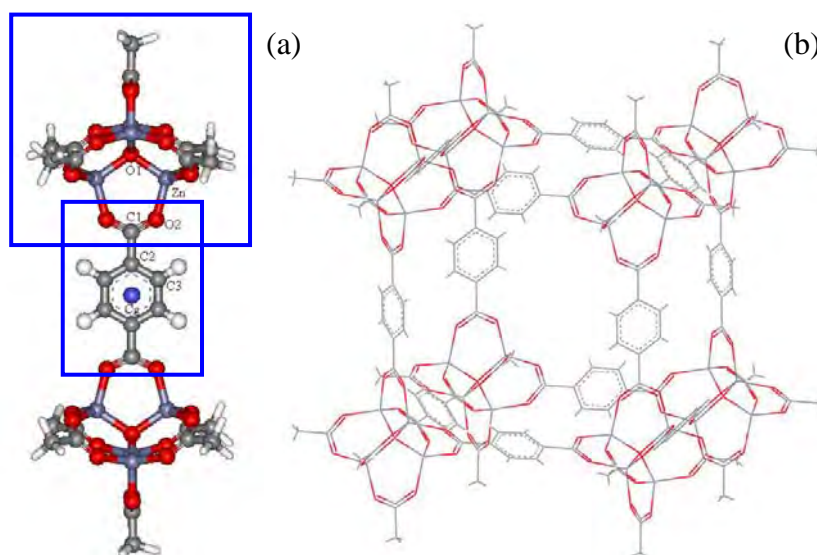
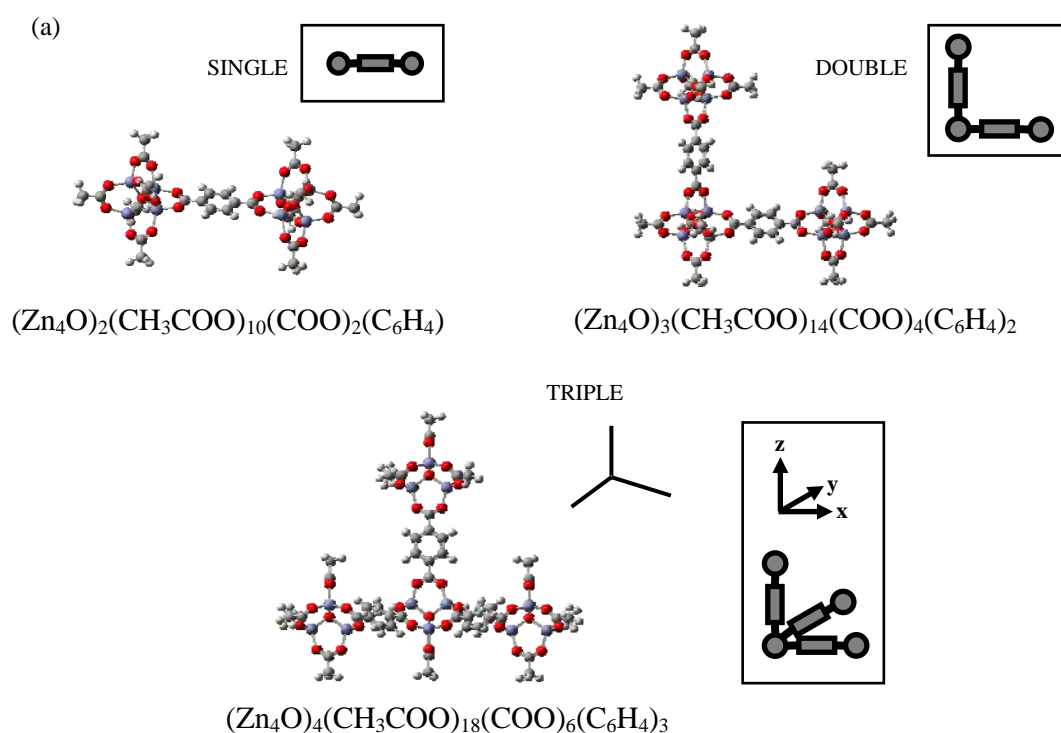


Figure 3.1 (a) A single fragment of MOF-5 consisting of two corners and one linker and (b) the whole MOF-5 unit cell which were generated as initial structure to be used in this study where C_g donates center of mass of the benzene ring.

3.1.2 The Models

Seeking for an optimal compromise between fragment size vs. the required computer time, different quantum mechanical methods and fragment sizes were examined. The MOF-5 was represented by the three models shown in Figure 3.2a. The fragments consisting of 1, 2 and 3 columns were named, for simplicity, as SINGLE, DOUBLE and TRIPLE, respectively.

For interaction at the linker, CO₂ was generated to move along the vector perpendicular to the molecular plane of the benzene ring at the C_g (see Figure 3.1a for definition). Here, two possible orientations of guest molecules were taken into account, parallel (||) and perpendicular (⊥) to the MOF fragments as shown in Figure 3.2b1. For the SINGLE model, the optimal C-C_g distant related with binding energy was searched with 2 steps. Firstly, C-C_g distant starts from 3 to 4 Å and 4 to 5 Å of || and ⊥ orientations, respectively with 0.1 Å of interval. Secondly, C-C_g distant was searched again with 0.01 Å of interval in range of first minimum binding energy from the first step. For the DOUBLE and TRIPLE models, calculations were carried out only for one wing of the fragments as same procedure as the SINGLE model. For the MOF corner, CO₂ molecule, also in the two configurations, was generated to move along the vector pointing to O1 (see Figure 3.1a) with the same procedure as the linker but different starting distance. Note that the vector denotes the C₃ symmetry axis of the three O1-Zn bonds of the corner.



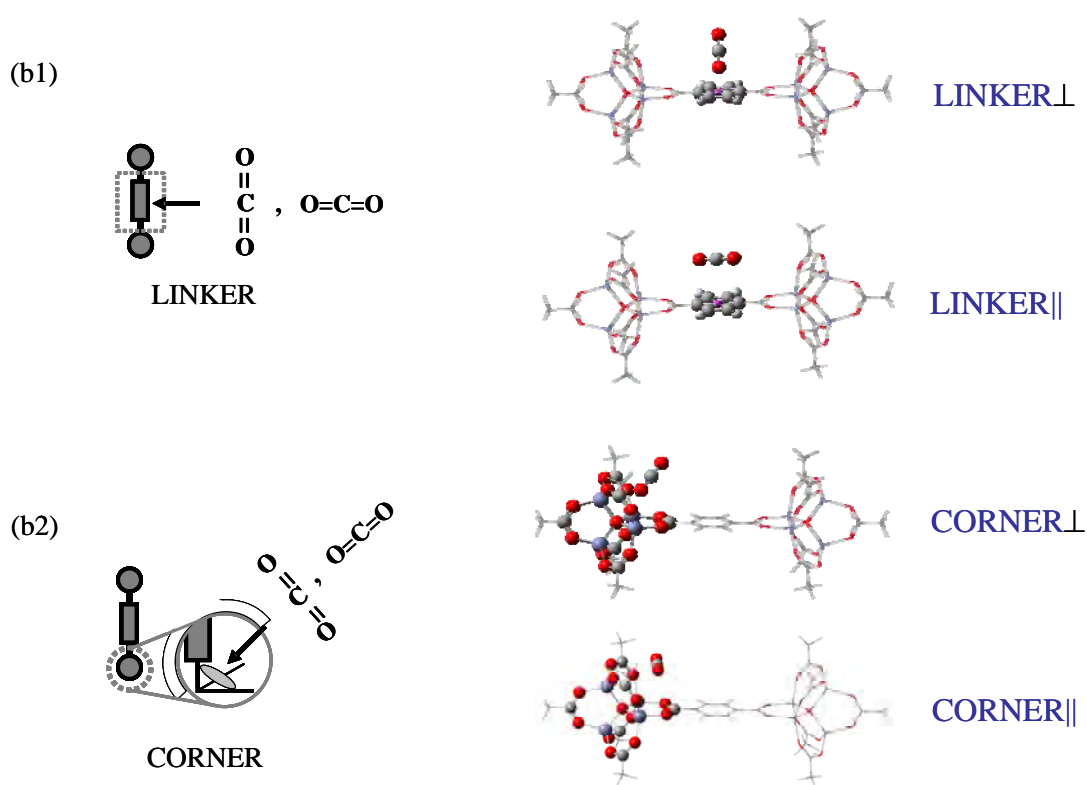


Figure 3.2 Representation of the calculation models where rectangular and filled-circle represent linker and corner, respectively, and dot-circle denotes the model part for which high level of accuracy in the ONIOM calculation was applied. (a) Models SINGLE, DOUBLE and TRIPLE represent the MOF fragments containing one, two and three units as oriented, where one unit of the model is composed of two corners connected by a linker (Figure 1a). Orientation of CO_2 molecule binds in parallel and perpendicular to the linker (b1) and corner (b2) binding sites.

3.1.3 ONIOM Calculations including BSSE

Referred to these three SINGLE, DOUBLE and TRIPLE models defined in section 3.1.2, the ONIOM interaction energy (ΔE_{ONIOM}) of each system is derived as

$$\Delta E_{\text{ONIOM}} = E_{(\text{real},\text{low})} + E_{(\text{model},\text{high})} - E_{(\text{model},\text{low})} \quad (3.1)$$

Where $E_{(\text{real,low})}$ is the total energy of the real system using the low level method, while $E_{(\text{model,high})}$ and $E_{(\text{model,low})}$ denote the total energies of the model part calculated with high and low level methods, respectively. The method used for the high : low levels was treated by MP2/6-31G** : HF/6-31G**. The high accurate (model) MP2/6-31G** part covers the compositions (C_6H_4) and $(\text{Zn}_4\text{O})(\text{CO}_2)_6$ for the linker and corner domains, respectively, labeled as dot-circles in Figure 3.2. Discrepancies due to an unbalance of the basis set used, known as basis set superposition error (BSSE) were examined and take into account for all data points reported in this study.

3.2 Molecular Dynamic Simulations

3.2.1 Initial Lattice Structure

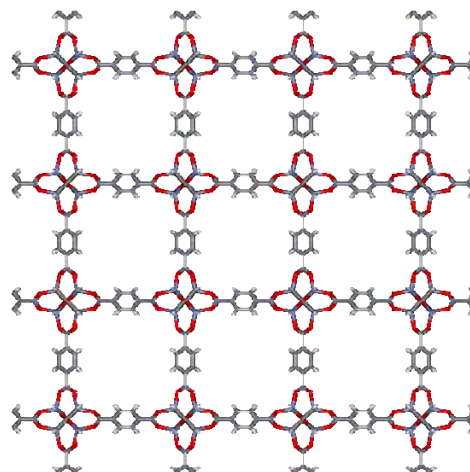


Figure 3.3 The $2 \times 2 \times 2$ unit cells of MOF-5 lattice structure used in the simulation.

The initial atomic coordinates of MOF-5 used in molecular dynamic simulation were taken from x-ray crystal structure [48], which has a cubic unit cell with $Fm\bar{3}m$ space group and lattice length of 25.8 Å, then, using it as prototype to build up 8 unit cells of MOF-5 in $2 \times 2 \times 2$ grid. The obtained simulation cube contains 3,392 atoms with the lattice length of 51.78 Å.

3.2.2 Force Field Parameters

CO₂ and MOF-5 were represented as rigid models, in which the intermolecular interaction between MOF-5 and CO₂ was calculated using Coulomb and Lennard-Jones pair potential. The L-J potential parameters of CO₂ consisting of 2 species of atom(x), where x represents C or O atom, were given by σ_x and ε_x/k_B . The parameters for Oxygen atom (O) ($\sigma_o=3.064$ Å and $\varepsilon_o/k_B = 82.997$ K) and carbon atom (C) ($\sigma_c=2.785$ Å and $\varepsilon_c/k_B = 28.999$ K) with C-O bond length of 1.161 Å were taken from the EPM model force field developed by Harris and Yung. [49] The partial charges are $+0.66450e$ on C atom and $-0.33225e$ on O atom. The MOF-5 structure containing 8 atom types were labeled in Figure 3.1a. Description of potential parameters for non-bonded interaction of MOF-5 were shown in Table 3.1 [26].

Table 3.1 Potential parameters for non-bonded interaction in MOF-5 [26].

Atom type	Definition	q (e)	σ (Å)	ε (kJ/mol)
Zn	zinc atom	1.200	2.3110	0.006
O1	Oxygen bonded to zinc	-1.200	3.0882	3.548
O2	Oxygen of carboxylate group	-0.600	2.9861	3.548
C1	carbon bonded to O2	0.600	3.6170	0.619
C2	carbon bonded to C1	0.000	3.6170	0.619
C3	carbon bonded to H	-0.100	3.6170	0.619
H	hydrogen bonded to C atom	0.100	2.4500	0.159

3.2.3 Molecular Dynamic Simulation Details

With 8 unit cell of MOF5 as described in 3.2.1, the simulations were carried out at 8, 64, 128, 256 and 512 molecules of CO₂ per simulation cube (MPC). In each system, the CO₂ loading was applied by random program. Periodical boundary condition was applied to avoid finite size effect. The simulations were performed with *NVT* ensemble which is suitable for rigid system [26]. The time step was 0.05 fs and the equilibration length of each run was 1 ps, corresponds to 1 ns of simulation time. The average temperature of the system was 300 K. All simulations were performed with DL_POLY 2 package [47].

CHAPTER IV

RESULTS AND DISCUSSION

4.1 Quantum Chemical Calculations

4.1.1 Geometries of the MOF-5

Starting from the two clusters, one column (Figure 3.1a) and the whole unit cell (Figure 3.1b) of the MOF-5, their intramolecular geometries (bond lengths and bond angles) were fully optimized using different methods and levels of accuracy. The results were summarized in Table 4.1.

Relative to experimental geometries [6], discrepancies were, as expected, found among the results obtained from different methods and basis sets used. The MPW1PW91/6-31G** geometries for the one column cluster are in excellent agreement with the experimental data. Due to the fact that the MPW1PW91/6-31G** is highly time consuming, it is practically impossible to apply it for the full unit cell cluster. Therefore, the optimal choice shifts to the next lower-accurate B3LYP/6-31G* and B3LYP/6-31G** methods. As shown in Table 4.1, no significant difference was found on the geometries of the clusters yielded from these two methods. Then B3LYP/6-31G** is sufficient method for geometry optimization. In previous study, the weak binding site is located on benzene ring at the linker. In this study, the sufficient method of binding energy calculation was observed at this position. However, the MP2/6-31G** binding energy (-2.70 kJ/mol) is slightly lower than that of MP2/6-31G* (-2.40 kJ/mol) although the time required is also slightly longer. Taking into account all the data mentioned earlier, the MP2/6-31G**, with BSSE corrections, was chosen to represent the high accurate part of the ONIOM calculation.

Note that the results yielded from the two clusters, one column and one unit cell, are in good agreement. This indicates that size of the one column cluster is sufficient to represent intramolecular geometries of the MOF-5. In addition, our results, especially Zn–O1 and Zn–O2 distances, are closer to the experimental data [5] in comparison to those reported in refs. 50, 51.

Table 4.1 Selected bond distances and bond angles obtained from the geometry optimizations for the two clusters shown in Figure 3.1 where the experimental data [6] and the other theoretical calculations [50,51] were also given for comparison (see Figure 3.1 for atomic labels).

method/basis set	bond length (pm)				Bond angle (°)		
	Zn-O ₁	Zn-O ₂	O ₂ -C ₁	C ₁ -C ₂	O ₁ -Zn-O ₂	Zn-O ₂ -C ₁	O ₂ -C ₁ -C ₂
<i>a. One column cluster (Figure 3.1a)</i>							
AM1	205.5	212.4	128.5	148.5	110.1	134.172	119.0
PM3	195.1	205.3	127.6	150.7	112.4	131.2	118.2
HF/6-31G*	197.8	196.9	124.5	149.7	110.1	132.8	117.7
HF/6-31G**	197.8	196.9	124.5	149.7	110.1	132.8	117.7
B3LYP/6-31G*	195.4	195.0	127.0	149.6	111.2	131.1	117.2
B3LYP/6-31G**	195.3	195.1	127.0	149.6	111.1	131.2	117.2
B3LYP/6-311G**	196.1	195.7	126.4	149.6	109.7	131.1	117.3
B3LYP/6-311G** [50]	197.2	195.3	126.2	151.0	110.8	131.7	117.8
GULP [50]	212.6	195.7	127.2	138.8		134.5	120.3
MPW1PW91/6-31G**	194.0	194.0	126.4	149.1	111.2	131.0	117.2
<i>b. One unit cell cluster (Figure 3.1b)</i>							
AM1	205.4	212.1	128.5	148.5	110.2	134.2	119.0
PM3	195.1	205.4	127.5	150.7	112.1	130.7	117.6
B3LYP/6-31G**	195.3	194.8	127.0	149.6	111.4	131.1	117.3
AM1 [51]	205.5	212.4	128.4	148.5	110.1	134.2	119.0
PM3 [51]	195.1	205.6	127.5	150.7	112.1	130.6	117.5
Experimental data	193.6	194.1	125.2	149.8	111.1	132.3	118.1

4.1.2 Effect of an Unbalance of the Basis Sets

Figure 4.1 and 4.2 show ONIOM binding energies with and without BSSE corrections between CO₂ in parallel (||) and perpendicular (⊥) configuration, respectively and the three clusters, SINGLE, DOUBLE and TRIPLE, of MOF-5.

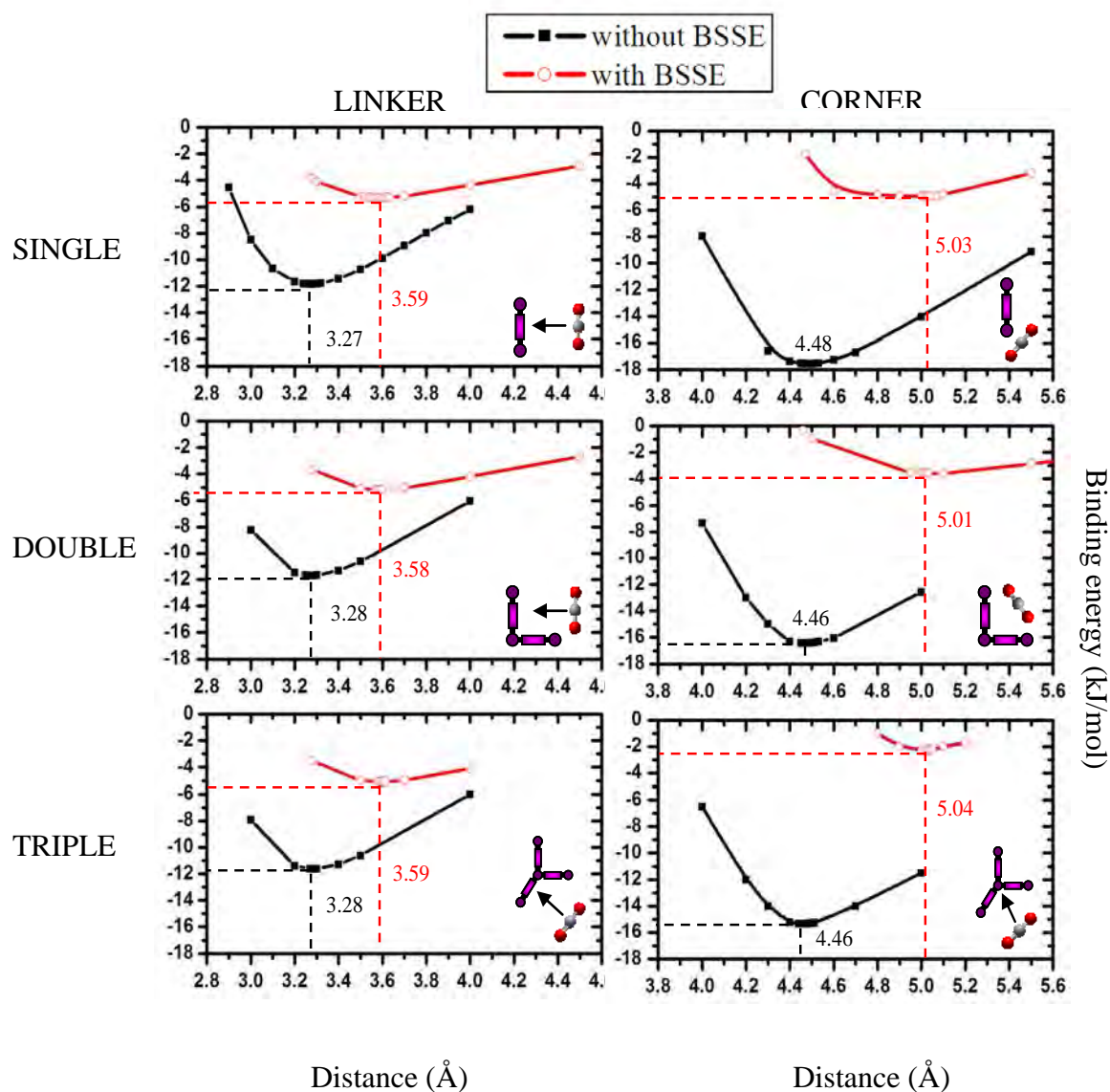


Figure 4.1 ONIOM binding energies with and without BSSE corrections for CO₂/MOF-5 in parallel (||) configuration for all systems. For the linker and corner calculations, the distances were measured from the C atom of CO₂ to Cg and O1, respectively.

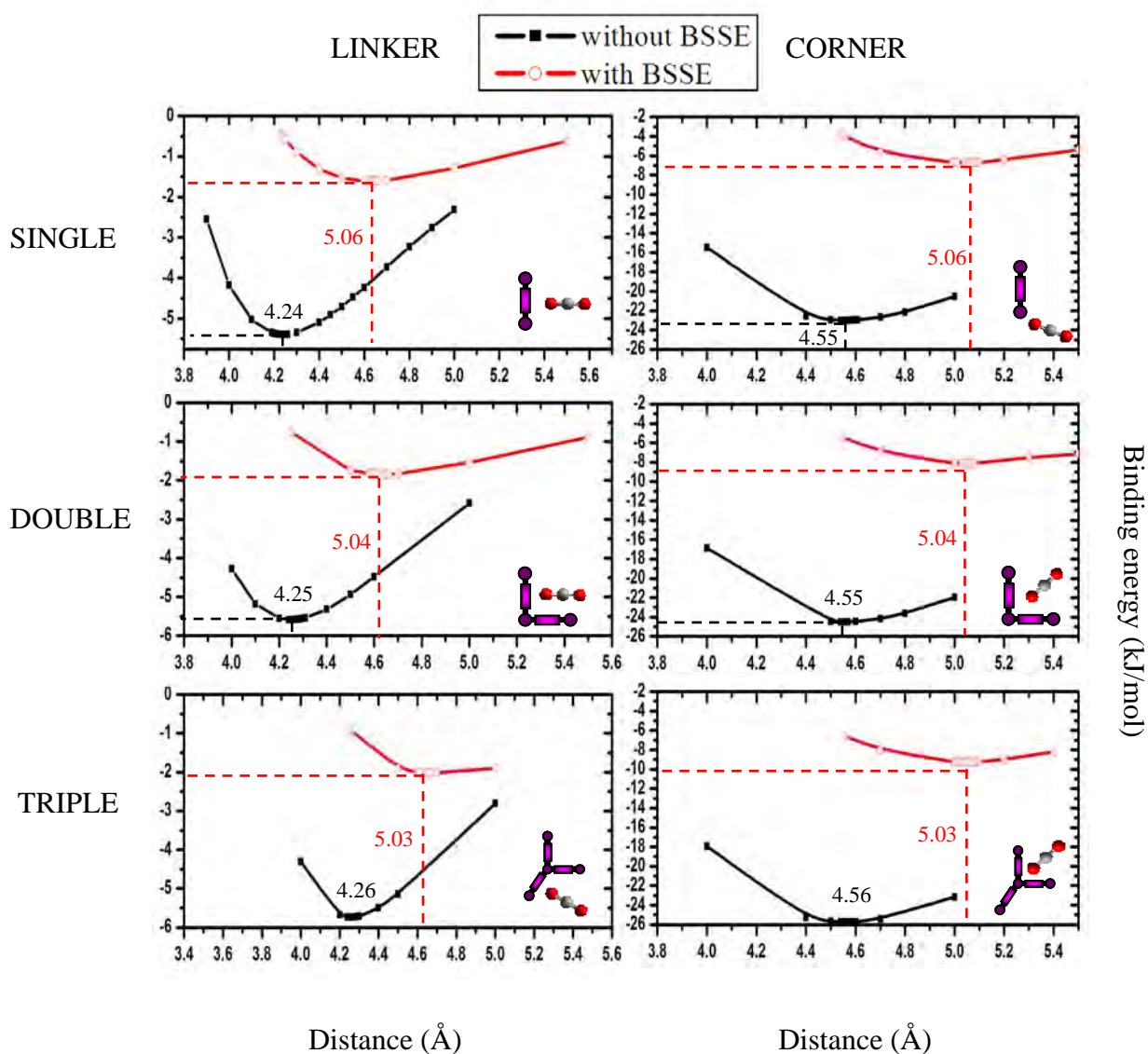


Figure 4.2 ONIOM binding energies with and without BSSE corrections for $\text{CO}_2/\text{MOF-5}$ in perpendicular (\perp) configuration for all systems. For the linker and corner calculations, the distances were measured from the C atom of CO_2 to Cg and O1, respectively.

It was surprisingly found from the plots that BSSE leads to dramatic changes of the calculated results. Distance to the minimum changes from 4.24 to 4.64 Å for the SINGLE LINKER \perp and from 4.55 to 5.06 Å for the SINGLE CORNER \perp clusters. The corresponding interaction energy differences for the linker and corner are 3.7 and 16 kJ/mol, respectively, shifted to weaker interactions. The observed results indicate obviously that the investigated systems requires BSSE corrections.

4.1.3 MOF-5 and CO₂ Binding

ONIOM binding energy between MOF-5 in the three cluster models, SINGLE, DOUBLE and TRIPLE (Figure 3.2a) and CO₂ molecule in the two orientations, || and ⊥, were calculated separately for the linker and corner parts (Figures 3.2b1 and 3.2b2) and summarized in Tables 4.2 and 4.3. The distances were measured from C_g (for linker) and O1 (for corner) to C atom of CO₂. The BSSE corrections were applied in all data points.

Considering the binding energies at the same configuration of guest molecules (|| or ⊥) at the linker part (Table 4.2). The difference was found for the CO₂ complexes of different cluster sizes, SINGLE, DOUBLE and TRIPLE. The cluster size effect was slightly found, *i.e.*, increasing of the MOF-5 cluster from SINGLE to TRIPLE leads to weaker binding energy (from -5.32 to -5.08 kJ/mol) for the || whereas this change was opposite (from -1.61 to -2.02 kJ/mol) for the ⊥ configurations. For the effects of molecular orientation, the binding energy of the || configuration for the CO₂/MOF-5 complexes is about three times more stable than that in the ⊥ configuration.

In contrast to what was observed for the linker, the calculated results at the MOF-5 corner (Table 4.3) lead to the following two main conclusions: (i) CO₂ prefers to approach O1 (defined in Figure 3.1b) at the corner of the MOF-5 in the ⊥ configuration, *i.e.*, the binding energies of the || configuration of -4.94, -3.55 and -2.25 kJ/mol are obviously less stable than those of the ⊥ configuration of -6.72, -8.14 and -9.27 kJ/mol, respectively. (ii) Effects of cluster size were found to be strong for the CO₂/MOF-5 complexes. As shown, an increasing of the cluster size from SINGLE to TRIPLE decreases the binding energy of the || configuration from -4.94 to -2.25 kJ/mol. In contrast, this change leads to an increasing of the binding energy of the ⊥ configuration from -6.72 to -9.27 kJ/mol. The detected data let us conclude that for CO₂, the minimum cluster size to represent the MOF corner must contain at least three SINGLE MOF units (see Figure. 3.2a).

Taking into account all the data discussed above for CO₂ molecules, interactions at the MOF's corner are stronger than those at the linker. This can be due to the fact that the interaction with the arene ring (see Fig. 3.1) of the linker unit is dominated by the dispersion forces. This is not the case for the MOF's corner where the interaction is influenced by electronic forces due to the (Zn₄O)₂(COOCH₃)₁₀ unit.

In summary, the optimal binding sites of guest molecules as well as their orientations in the cavity of the MOF-5 based on the binding energies shown in Table 4.2 and 4.3 are CORNER \perp for CO₂ complexes. In addition, the binding energies of the MOF-5 with the CO₂ molecule complex are in the following order: CO₂: CORNER \perp < LINKER \parallel < CORNER \parallel < LINKER \perp .

Table 4.2 ONIOM binding energies with BSSE corrections and the corresponding distances between Cg point of MOF-5 in the three cluster models (SINGLE, DOUBLE and TRIPLE in figure 3.2a) and CO₂ in two orientations (\parallel and \perp) in which the distance was measured from Cg of linker to C atom of CO₂.

Model		Distance Cg-C (Å)	Binding energy (kJ/mol)
MOF-5	Orientation		
SINGLE	\parallel	3.59	-5.32
	\perp	4.64	-1.61
DOUBLE	\parallel	3.58	-5.16
	\perp	4.65	-1.84
TRIPLE	\parallel	3.59	-5.08
	\perp	4.66	-2.02

Table 4.3 ONIOM binding energies with BSSE corrections and the corresponding distances between Cg point of MOF-5 in the three cluster models (SINGLE, DOUBLE and TRIPLE in figure 3.2a) and CO₂ in two orientations (|| and ⊥) in which the distance was measured from O1 of corner to C atom of CO₂.

Model		Distance O1-C (Å)	Binding energy (kJ/mol)
MOF-5	Orientation		
SINGLE		5.03	-4.94
	⊥	5.06	-6.72
DOUBLE		5.01	-3.55
	⊥	5.04	-8.14
TRIPLE		5.04	-2.25
	⊥	5.03	-9.27

4.2 Molecular Dynamic Simulations

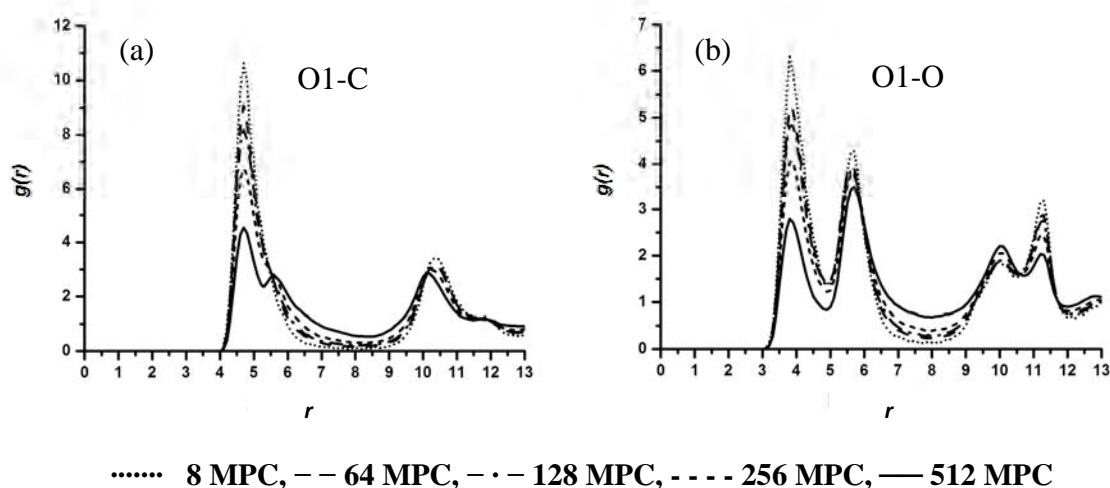
4.2.1 Structure of CO₂ at the MOF-5 Corner

To monitor structural data of CO₂ in MOF-5, atom-atom radial distribution functions (RDF), expressed as $g_{ij}(r)$, the probability of finding a particle of type j in a sphere of radius, r , around a particle of type i , were calculated. The MOF-CO₂ RDFs were evaluated separately for all systems where i denotes O1 of MOF-5 and middle of the benzene ring of the MOF-5 linker (Cg that generated as an average of the coordinates of the 6 carbon atoms of the benzene ring) and j is C and O atoms of CO₂ (see Figure 3.1 for atomic labels). The corresponding O1-C, O1-O, Cg-C and Cg-O RDFs were given in Figures 4.3 and 4.4. In addition, distribution of the corresponding coordination number calculated up to the first minimum of the O1-O and the Cg-O RDFs were also examined and plotted in Figures 4.3c and 4.4c, respectively.

Characteristics of CO₂ adsorption at the MOF-5 corner can be understood from the O1-C and O1-O RDFs (Figures 4.3a and 4.3b). The plots for all concentrations of the O1-C and O1-O RDFs show a first sharp peak centered at 4.70 Å and 3.82 Å, respectively. This indicates that CO₂ adsorbs firmly to the MOF-5

corner in which the average distances from O1 of MOF-5 (see Figure 3.1 for definition) to C and O atoms of CO₂ are 4.70 Å and 3.82 Å, respectively. The two peaks of the O1-O RDFs centered at 3.82 Å and 5.70 Å denote the distances from O1 to the two oxygen atoms of CO₂ whereas the distance between the two maxima of 1.88 Å is approximately the same as that of the length of the CO₂ molecule (2.32 Å). This feature suggests us to preliminary conclude that CO₂ points, somehow, its molecular axis to the MOF-5 corner, O1 atoms. Precise orientations of the CO₂ was calculated and discussed again in section 4.2.3. Interest is focused to the O1-C RDF for the loading of 256 MPC shown in Figure 4.3b where the RDF shoulder at ~5.6 Å starts to be detected. This shoulder is more pronounce at 512 MPC whereas position of the first peak remains unchanged, compared to the other concentrations. This indicates a structural formation of the CO₂ in the MOF-5 cavity. More details investigations and discussions were given in the next section.

To examine number of CO₂ molecules coordinated to the MOF-5 corner, the results were displayed in Figure 4.3c in terms of their distributions, evaluated up to the first minimum of 4.90 Å of the O1-O RDFs of the five concentrations. The plots represent number of the first O atom of CO₂ molecules lying under the first peak centered at 3.82 Å of the O1-O RDF (Figure 4.3a). Broad distribution of the coordination numbers shown in Figure 4.3c as well as non-zero of the peak height at the first minimum of the O1-O RDF indicates weak interactions of CO₂ at the MOF-5 corner and mobility of the coordinated CO₂ molecules lying under the first two peaks of the O1-O RDF, respectively. As expected, the average coordination number was observed to increase as a function of loading, from 0.07 to 0.6, 1.2, 2.2 and 2.9 CO₂ molecules when the loading increases from 8 to 64, 128, 256 and 512 MPC.



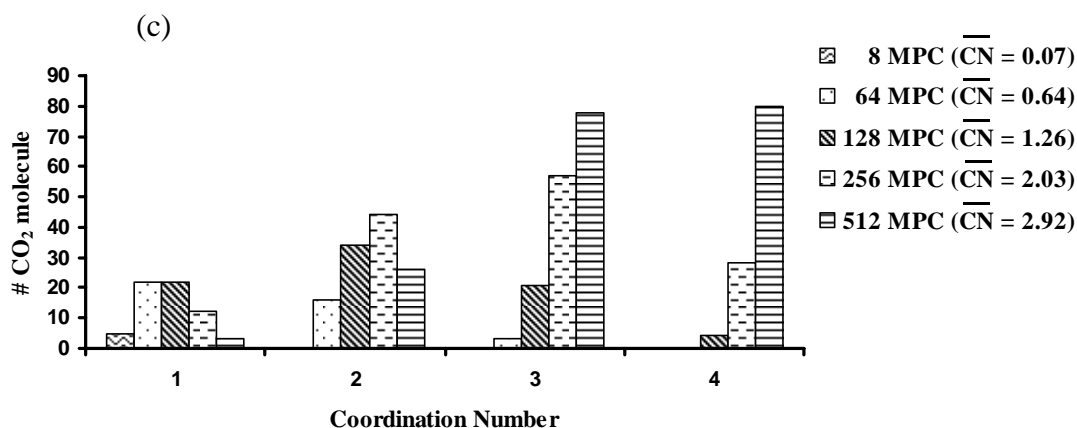


Figure 4.3 (a)-(b) Radial distribution functions (RDF) for the 5 loadings of CO₂, centered at O1 of MOF-5 (see Figure 1 for atomic labels) to O and C atoms of CO₂, respectively. (c) Distribution of the corresponding coordination number calculated up to the first minimum of 4.90 Å of the O1-O RDF where the average coordination numbers ($\overline{\text{CN}}$) were also shown.

4.2.2 Structure of CO₂ at the MOF-5 Linker

As defined above, the Cg-C and Cg-O RDFs representing the distribution of C and O atoms of CO₂ around the Cg (center of the benzene ring) of the MOF-5 linker were calculated and plotted in Figures 4.4a and 4.4b, respectively. Here, distribution of the corresponding coordination number calculated up to the first minimum of 6.00 Å of the Cg-O RDF (Figure 4.4a) were shown in Figure 4.4c.

The Cg-C and Cg-O RDFs for all concentrations show sharp first peak at 4.76 Å and 5.25 Å, respectively. An apparent of the two maxima of the two RDFs at almost the same distance indicate free orientation of the CO₂ coordinated to the MOF-5 linker. This conclusion was also supported by an emerge of single Cg-O peak due to the two oxygen atoms of CO₂ molecule. Because of such weakly binding, not much structural data can be extracted from these RDFs.

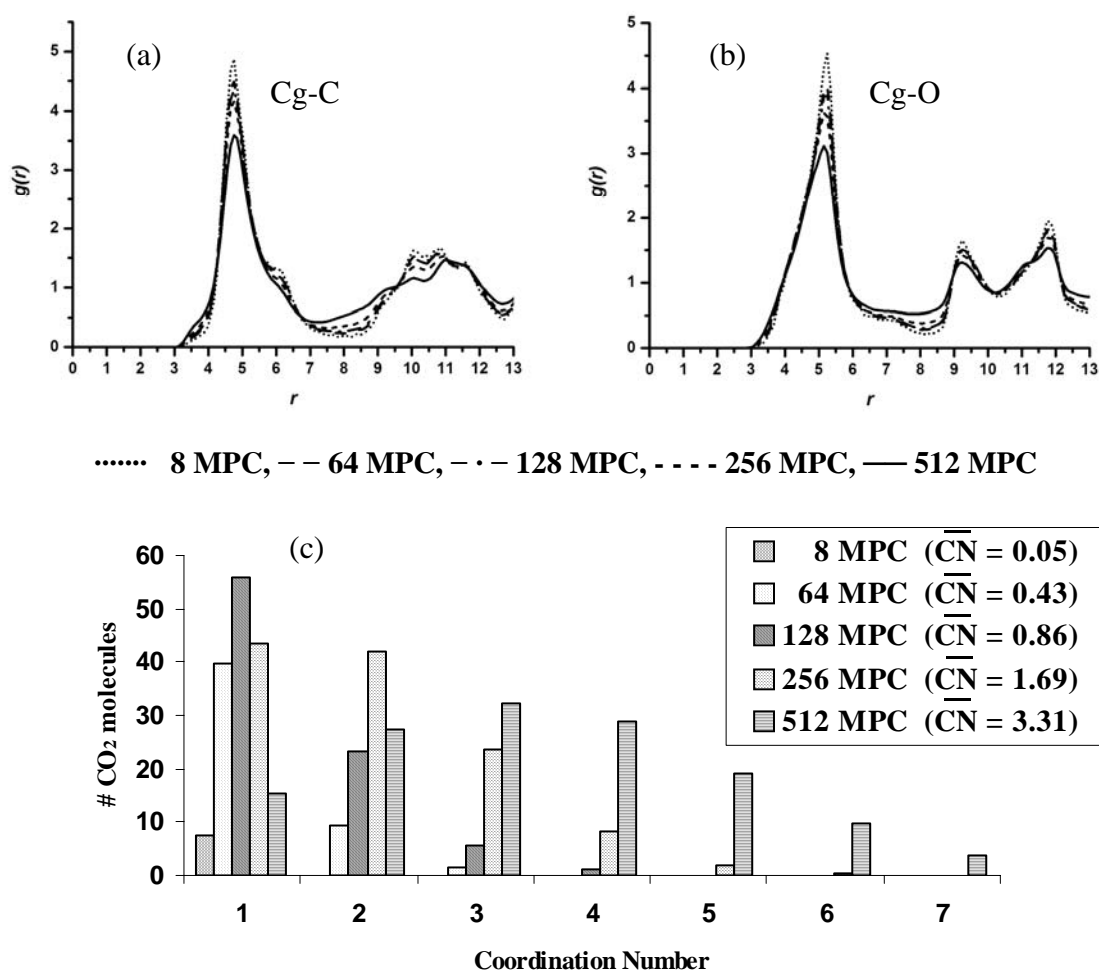


Figure 4.4 (a)-(b) Radial distribution functions (RDF) for the 5 loadings of CO₂, centered at the middle of benzene ring of the MOF-5 linker, Cg (see text for definition), to O and C atoms of CO₂, respectively. (c) Distribution of the corresponding coordination number averaged up to the first minimum of 6.00 Å of the Cg-O RDF where the average coordination numbers (\overline{CN}) were also shown.

4.2.3 Orientation of CO₂ Around the MOF-5 Binding Site

To visualize orientation of CO₂ which coordinate to the corner and the linker binding sites, distribution of the angle θ , defined by the three atoms O1-O-C, was evaluated. Here, O1 still denote the MOF-5 atom (Figure 3.1) while O and C are the two atoms of CO₂. The plots for all concentrations were given in Figure 4.5a for the CO₂ lying under first peak of the O1-O RDF ($0.0 \text{ \AA} \leq r \leq 4.90 \text{ \AA}$) except 512 MPC

was plotted with $0.0 \text{ \AA} \leq r \leq 6.50 \text{ \AA}$ under 2 peaks. For the loading of 512 MPC, the results were also plotted separately again (Figure 4.5b) for the CO_2 located under the first peak ($0.0 \text{ \AA} \leq r \leq 5.20 \text{ \AA}$) and the second peak ($5.20 \text{ \AA} < r \leq 6.50 \text{ \AA}$) of the O1-C RDF (maximum and minimum limits of r were assigned regarding the minima of the focused peaks shown in Figure 4.2). In addition, the same plots were given in Figure 4.5c for the CO_2 coordinated to the MOF-5 linker (locate under the first peak of the Cg-O RDF at $0.0 \text{ \AA} \leq r \leq 6.00 \text{ \AA}$) where the angle ϕ was defined by the Cg-O-C atoms.

Exclude the loading of 512 MPC, the distribution plots for all concentrations of the MOF-5 corner representing orientation of the CO_2 lying within the first peaks of the O1-O RDF show two maxima at $\theta = \sim 35^\circ$ and $\sim 130^\circ$. This indicates orientation of the nearest neighbors of O1, and hence the MOF-5 corner, in the manner to tilt their molecular axis by 35° to 50° (180° - 130° due to the second peak) from the O1-C axis (see also an inset of Figure 4.5a). Interest is focused to the distribution plots for the 512 MPC as shown in Figure 4.5b. This is in connection with the change of the structural property in which the RDF for the 512 MPC loading was found to form pronounced shoulder at $\sim 5.6 \text{ \AA}$ (Figure 4.3a). Whereas the two pronounced peaks at $\theta = \sim 35^\circ$ and $\sim 130^\circ$ (solid line of Figure 4.5b) which are the characteristic of the nearest neighbors remain unchanged, the other peak at $\sim 80^\circ$ (dot line in Figure 4.5b) was additionally yielded. The newly detected peak indicates the formation of another layer of CO_2 (located under the shoulder of the O1-C RDF) which aligns their molecular axis perpendicular to the O1-C axis. The observed data suggest us to conclude that the CO_2 lying in this layer behave as the first shell coordination numbers of the CO_2 located under the O1-C RDF first peak. Simultaneously, they are also proposed to coordinate weakly to fill in the rest space around the MOF-5 corner. Note that the distance of $\sim 0.9 \text{ \AA}$ from the first peak (at 4.70 \AA) to its shoulder (at $\sim 5.6 \text{ \AA}$) of the O1-C RDF (Figure 4.3a) is too short to claim that this layer of CO_2 is the second coordination shell of O1.

For the MOF-5 linker, the plots for all concentrations show broad distribution ranging from 0° to 180° with the maxima at $\phi = \sim 80^\circ$ (Figure 4.5c). This indicates a free orientation of the CO_2 molecules which coordinate to the MOF-5 linker. Although the favorite alignment is to point their molecular axis perpendicular to the Cg-O axis (an inset of the Figure).

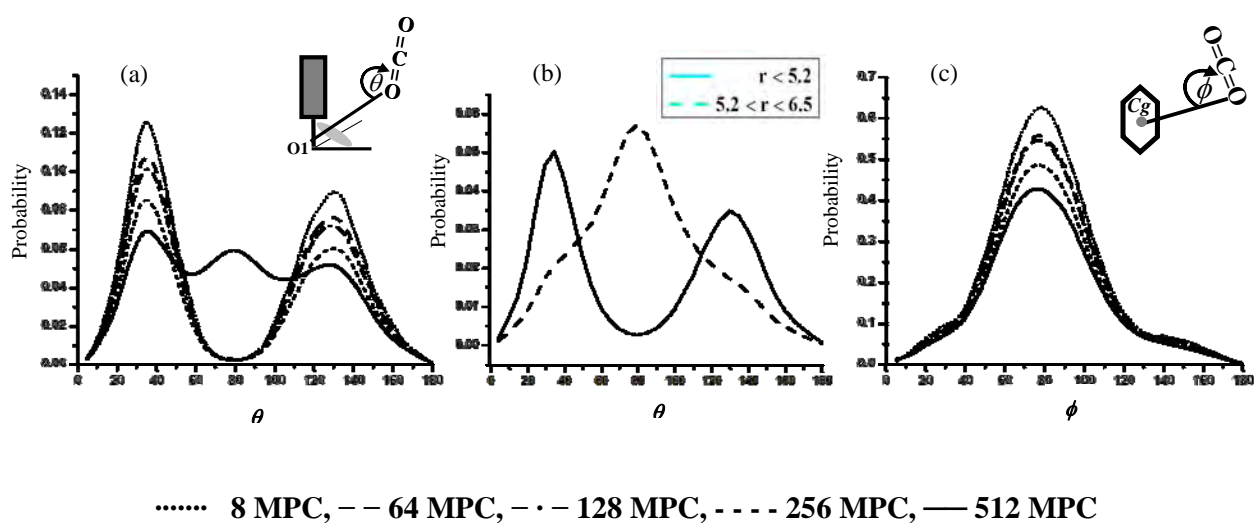


Figure 4.5 Distribution of the angles θ and ϕ representing orientation of CO_2 lying under the first peak of the O1-O RDF (a) and the Cg-O RDF (c) where the plots for the 2 peaks of the O1-C RDF at the loading of 512 MPC was given separately (b) (see text for more details).

4.2.4 CO_2 - CO_2 Radial Distribution Functions

Figures 4.6a and 4.6b, the RDFs centered at C atom of one CO_2 to C and O atoms of the other CO_2 were monitored and represented as C-C and C-O, respectively. As can be clearly seen, no significant difference was found in terms of the peak position. The C-C RDFs for all concentrations show sharp first peak at 4.13 Å indicating structural formation of CO_2 clusters in the MOF-5 cavity. Due to a weak interaction between the CO_2 molecules, therefore, preferential orientation can not be formed, and hence, no sharp peaks were found for the C-O RDF. In addition, the average coordination numbers of CO_2 for the loadings of 8 to 64, 128, 256 and 512 MPCs calculated up to the first minimum of 5.50 Å of the C-C RDF are 1.02, 1.14, 1.27, 1.67 and 2.76 molecules, respectively.

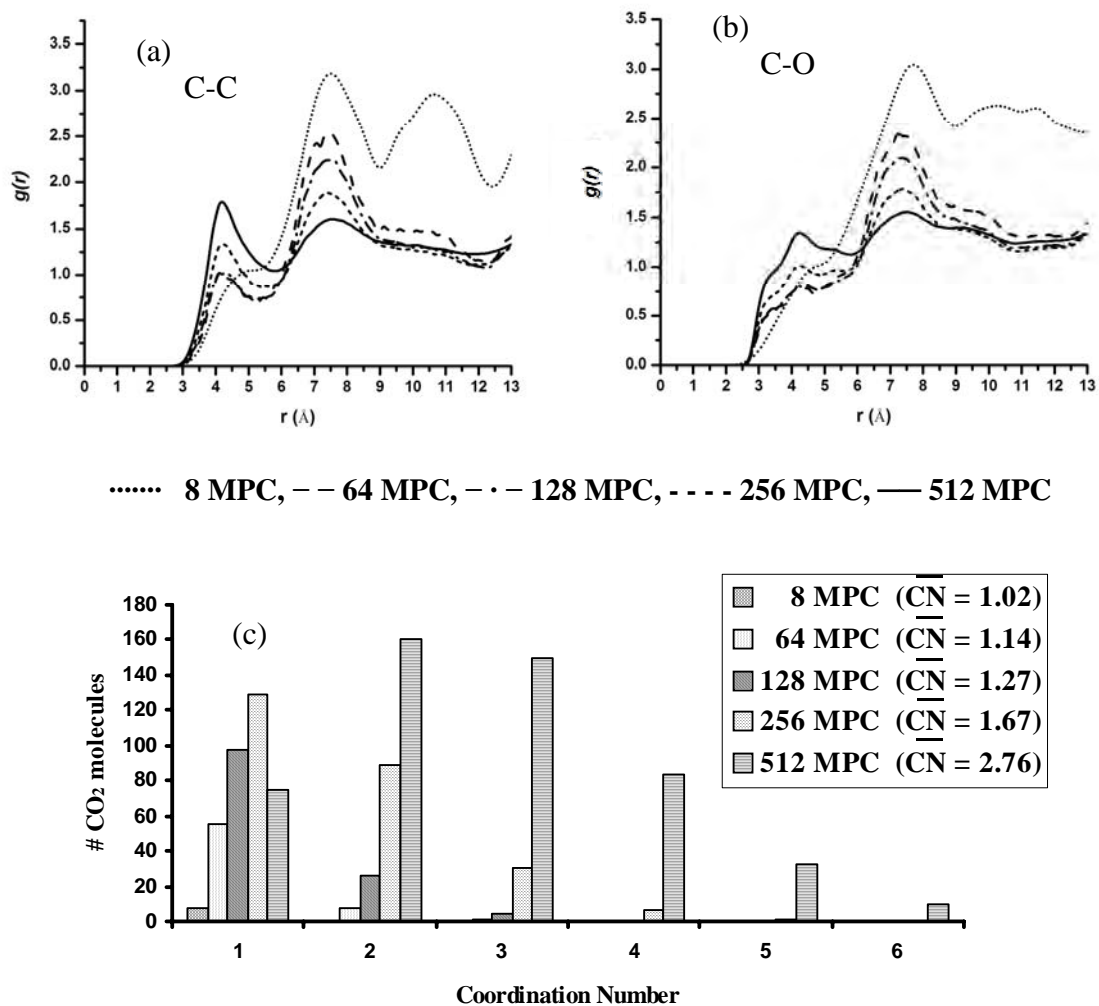


Figure 4.6 (a)-(b) C-C and C-O Radial distribution functions (RDF) for the 5 loadings of CO₂. (c) Distribution of the corresponding coordination number averaged up to the first minimum of 5.50 Å of the C-C RDF where the average coordination numbers (\overline{CN}) were also shown.

CHAPTER V

CONCLUSIONS

Quantum chemical calculations were carried out to examine the optimal binding site and orientation as well as the binding energy of CO₂ molecule in the cavity of MOF-5. CO₂ molecule was assigned to lie in the configurations parallel (||) and perpendicular (⊥) to the linker (LINKER) and corner (CORNER) domains. The ONIOM (MP2/6-31G** : HF/6-31G**) method was found to be a compromise between the accuracy and computer time required for the investigated system. Unbalance of the basis set used, known as basis set superposition errors (BSSE), was found to effect the calculated results, both binding distance and energy, significantly. However, the results indicate that the minimum cluster size to represent the MOF corner must contain at least one corner of (Zn₄O)(COO)₆ and three edges of ((Zn₄O)(COO)₆(C₆H₄))₃ unit in perpendicular orientation of CO₂ and the optimal binding site for the CO₂ molecule is at the MOF corner. In addition, it prefers to approach the corner by using its molecular axis moving along the C₃-symmetry axis of the corner of the MOF unit cell. The obtained BSSE corrected binding energy is -9.27 kJ/mol.

In the second part, molecular dynamic simulations of 2×2×2 lattice units of MOF-5 with the loading of 8, 64, 128, 256 and 512 molecules of CO₂ per simulation cube (MPC) were performed at 300 K. The obtained results are in agreement with those found from ONIOM calculations that CO₂ prefers to absorb at the MOF-5 corner site. To visualize orientation of CO₂ which coordinate to the corner and the linker binding sites, distribution of the angle θ , defined by the three atoms O1-O-C, was evaluated, where O1 denotes oxygen atom at the MOF corner, O and C are the two atoms of CO₂. Exclude the loading of 512 MPC, the distribution plots for all concentrations of the MOF-5 corner take place at $\theta = \sim 35^\circ$ and $\sim 130^\circ$. Interestingly, conclusion at MPC=512, the CO₂ was also found to form second layer coordinated where the corresponding $\theta = 90^\circ$. The observed data suggest us to conclude that the CO₂ lying in this layer behave as the first shell coordination numbers of CO₂ located in the first layer (where $\theta = \sim 35^\circ$ and $\sim 130^\circ$). Simultaneously, they are also proposed to coordinate weakly to fill the rest space around the MOF-5 corner as the second

layer. For the MOF-5 linker, the result indicates free orientation of the CO₂ molecules. The average coordination numbers of CO₂ at the corner and the linker sites are 2.9 and 3.1 molecules, respectively.

REFERENCES

- [1] Martin Cinke, Jing Li, Charles W. Bauschlicher Jr., Alessandra Ricca and Meyya Meyyappan. CO₂ adsorption in single-walled carbon nanotubes. *Chem. Phys. Lett.* 376(2003): 761–766.
- [2] Pragati Galhotra, Juan G. Navea, Sarah C. Larsen and Vicki H. Grassian. Carbon dioxide (C¹⁶O₂ and C¹⁸O₂) adsorption in zeolite Y materials: effect of cation, adsorbed water and particle size. *Energy Environ. Sci.* 2(2009): 401–409.
- [3] Krista S. Walton, Morgan B. Abney, M. Douglas LeVan. CO₂ adsorption in Y and X zeolites modified by alkali metal cation exchange. *Microporous Mesoporous Mater.* 91(2006): 78–84.
- [4] Andrew R. Millward and Omar M. Yaghi. Metal-organic frameworks with exceptionally high capacity for storage of carbon dioxide at room temperature. *J. Am. Chem. Soc.* 127(2005): 17998–17999.
- [5] Krista S. Walton, Andrew R. Millward, David Dubbeldam, Houston Frost, John J. Low, Omar M. Yaghi and Randall Q. Snurr. Understanding inflections and steps in carbon dioxide adsorption Isotherms in metal-organic frameworks. *J. Am. Chem. Soc.* 130(2008): 406–407.
- [6] Hailian Li, Mohamed Eddaoudi, Michael O’Keeffe and Omar M. Yaghi. Design and synthesis of an exceptionally stable and highly porous metal-organic framework. *Nature* 42(1999): 276–279.
- [7] Nathaniel L. Rosi, Juergen Eckert, Mohamed Eddaoudi, David T. Vodak, Jaheon Kim, Michael O’Keeffe and Omar M. Yaghi. Hydrogen Storage in Microporous Metal-Organic Frameworks. *Science* 300(2003): 1127–1129.
- [8] Nathaniel L. Rosi, Mohamed Eddaoudi, Jaheon Kim, Michael O’Keeffe and Omar M. Yaghi. Advances in the chemistry of metal–organic frameworks. *Cryst. Eng. Comm.* 4(2002): 401–404.
- [9] Mohamed Eddaoudi, Jaheon Kim, Nathaniel Rosi, David Vodak, Joseph Wachter, Michael O’Keeffe, Omar M. Yaghi. Systematic Design of Pore Size and Functionality in Isoreticular MOFs and Their Application. *Science* 295(2002): 469–472.
- [10] Ulrich Mueller, Markus M. Schubert, Friedhelm Teich, Hermann Pütter, Kerstin Schierle-Arndt and Joerg Pastre’. Metal–organic frameworks—prospective industrial applications. *J. Mater. Chem.* 16(2006): 626–636.

- [11] Marco Michelotti, Angelina Altomare, Francesco Ciardelli and Eckehart Roland. Zeolite supported polymerization catalysts: Copolymerization of ethylene and α -olefins with metallocenes supported on HY zeolite. *J. Mol. Catal. A: Chem.* 129(1998): 241–248.
- [12] Karl-Petter Lillerud, Mats Tilset, Unni Olsbye, Kai C. Szeto, Morten Bjorgen, Kjell Ove Kongshaug, Silvia Bordiga, Jasmina Hafizovic, Alexander Krivokapic, Soren Jakobsen. Metal-organic framework catalysts and their use in hydrocarbon transformation. USPTO Patent Application 20080306315.
- [13] Jorge Gascon, Ugur Aktay, Maria D. Hernandez-Alonso, Gerard P.M. van Klink, Freek Kapteijn. Amino-based metal-organic frameworks as stable, highly active basic catalysts. *J. Catal.* 261(2009): 75–87.
- [14] Seda Keskin and David S. Sholl. Assessment of a metal organic framework membrane for gas separations using atomically detailed calculations: CO₂, CH₄, N₂, H₂ mixtures in MOF-5. *Ind. Eng. Chem. Res.* 48(2009): 914–922.
- [15] Banglin Chen, Chengdu Liang, June Yang, Damacio S. Contreras, Yvette L. Clancy, Emil B. Lobkovsky, Omar M. Yaghi and Sheng Dai. A microporous metal organic framework for gas chromatographic separation of alkanes. *Angew. Chem. Int. Ed.* 45(2006): 1390–1393.
- [16] Anja Car, Chrtomir Stropnika, Klaus-Viktor Peinemann. Hybrid membrane materials with different metal-organic frameworks (MOFs) for gas separation. *Desalination* 200(2006): 424–426.
- [17] Jesse Rowsell and Omar M. Yaghi. Strategies for Hydrogen Storage in Metal-Organic Frameworks. *Angew. Chem. Int. Ed.* 44(2005): 4670–4679.
- [18] Jaheon Kim, Banglin Chen, Theresa M. Reineke, Hailian Li, Mohamed Eddaoudi, David B. Moler, Michael O’Keeffe and Omar M. Yaghi. Assembly of metal organic frameworks from large organic and inorganic secondary building units: new examples and simplifying principles for complex structures. *J. Am. Chem. Soc.* 123(2001): 8239–8247.
- [19] Tina Düren, Lev Sarkisov, Omar M. Yaghi and Randall Q. Snurr. Design of new materials for methane storage. *Langmuir* 20(2004): 2683–2689.
- [20] Claudia F. Braga and Ricardo L. Longo. Structure of functionalized porous metal-organic frameworks by molecular orbital methods. *THEOCHEM* 716(2005): 33–38.
- [21] Qingyuan Yang and Chongli Zhong. Molecular simulation of adsorption and diffusion of hydrogen in metal organic frameworks. *J. Phys. Chem. B.* 109(2005): 11862–11864.

- [22] Sanyue Wang, Qingyuan Yang and Chongli Zhong. Molecular simulation study of separation of CO₂ from alkanes using metal organic frameworks. *J. Phys. Chem. B.* 110(2006): 26507–26507.
- [23] Qingyuan Yang and Chongli Zhong. Molecular simulation of carbon dioxide methane hydrogen mixture adsorption in metal organic frameworks. *J. Phys. Chem. B.* 110(2006): 17776–17783.
- [24] Jonathan L. Belof, Abraham C. Stern, Mohamed Eddaoudi, and Brian Space. On the mechanism of hydrogen storage in a metal organic framework material. *J. Am. Chem. Soc.* 129(2007): 15202–15210.
- [25] Qingyuan Yang, Chongli Zhong and Jianfeng Chen. Computational Study of CO₂ Storage in Metal Organic Frameworks. *J. Phys. Chem. C.* 112(2008): 1562–1569.
- [26] Jeffery A. Greathouse and Mark D. Allendorf. Force field validation for molecular dynamics simulations of IRMOF-1 and other isorecticular zinc carboxylate coordination polymers. *J. Phys. Chem. C.* 112(2008): 5795–5802.
- [27] Michael Mueller. *Fundamentals of quantum chemistry: Molecular spectroscopy and modern electronic structure computations.* Kluwer Academic Publishers, 2002.
- [28] Errol Lewars. *Computational chemistry: Introduction to the Theory and Applications of Molecular and Quantum Mechanics.* Kluwer Academic Publishers, 2003.
- [29] Erwin Schrödinger. Quantisierung als eigenwertproblem. (Erste Mitteilung.). *Ann. Phys.* 79(1926): 361–376.
- [30] Christopher J. Cramer. *Essential of computational chemistry.* John Wiley & Sons Ltd., 2002.
- [31] Warren J. Hehre. *A Guide to molecular mechanics and quantum chemical calculations.* Wavefunction, Inc., 2003
- [32] Attila Szabo and Neil S. Ostlund. *Modern quantum chemistry.* McGraw-Hill Inc., 1989.
- [33] Robert G. Parr and Weitao Yang. *Density functional theory of atoms and molecules.* Oxford University Press, New York, 1989.
- [34] Chengteh Lee, Weitao Yang, and Robert G. Parr. Development of the Colle-Salvetti correlation-energy formula into a functional of the electron density. *Phys. Rev.* 37(1988): 785–789.
- [35] Axel D. Beck. Density-functional thermochemistry. III. The role of exact exchange. *Chem. Phys.* 98(1993): 5648–5652.

- [36] Møller C., Milton S. Plesset. Note on an Approximation Treatment for Many-Electron Systems. *Phys. Rev.* 46(1934): 618–622.
- [37] Matthew L. Leininger, Wesley D. Allen, Henry F. Schaefer and C. David Sherrill. Is Moller–Plesset perturbation theory a convergent ab initio method?. *J. Chem. Phys.* 112(200): 9213–9222.
- [38] Frank Jensen. *Introduction to computational chemistry. 2nd ed.*, John Wiley & Sons Ltd., 2007.
- [39] Per Olof Aastrand, Anders Wallqvist, and Gunnar Karlstroem. On the basis set superposition error in the evaluation of water dimer interactions. *J. Phys. Chem.* 95(1991): 6395–6396.
- [40] Stéphane Humbel, Stefan Sieber and Keiji Morokuma. The IMOMO method: Integration of different levels of molecular orbital approximation for bromery optimization of large systems: Test for n-butane conformation and sn2 reaction: RCl^+Cl^- . *J. Chem. Phys.* 105(1996): 1959–1967.
- [41] Mats Svensson, Stéphane Humbel, Robert D. J. Froese, Toshiaki Matsubara, Stefan Sieber, and Keiji Morokuma. ONIOM: A multilayered integrated MO MM method for geometry optimizations and single point energy predictions. A test for diels alder reactions and $\text{Pt}(\text{P}(t\text{-Bu})_3)_2 + \text{H}_2$ oxidative addition. *J. Phys. Chem.*, 100(1996): 19357–19363.
- [42] Keiji Morokuma, “ONIOM and its applications to material chemistry and catalyses. *Bull. Kor. Chem. Soc.* 24(2003): 697–801.
- [43] David C. Young. *Computational Chemistry: A Practical Guide for Applying Techniques to Real-World Problems.* John Wiley & Sons, Inc., 2001.
- [44] Andrew R. Leach. *Molecular modelling principle and application.* Pearson education Ltd., 2001.
- [45] Alan Hinchliffe. *Modelling molecular structures.* John Wiley & Sons, Inc., 2000.
- [46] Michael J. Frisch, et al. Gaussian 03, Revision C.02; Wallingford CT: Gaussian, Inc., 2004.
- [47] Bill Smith and Tim Forester. DL_POLY_2.0: A general-purpose parallel molecular dynamics simulation package. *J. Mol. Graphics* 14(1996):136-141.
- [48] Jesse L. C. Rowsell, Elinor C. Spencer, Juergen Eckert, Judith A. K. Howard, Omar M. Yaghi. Gas adsorption sites in a large-pore metal-organic framework. *Science* 309(2005): 1350–1354.

- [49] Jonathan G. Harris, and Kwong H. Yung. Carbon dioxide's liquid-vapor coexistence curve and critical properties as predicted by a simple molecular model. *J. Phys. Chem.* 99(1995): 12021–12024.
- [50] Baoling Huang, Alan J.H. McGaughey, Massoud Kaviany. Thermal conductivity of metal-organic framework 5 (MOF-5): Part I. Molecular dynamics simulations. *Int. J. Heat Mass Transfer* 50(2007): 393–404.
- [51] Claudia F. Braga, Ricardo L. Longo. Structure of functionalized porous metal-organic frameworks by molecular orbital methods. *THEOCHEM* 716(2005): 33–38.

APPENDICES

Appendix A:

PUBLICATION

The optimal binding sites of CH₄ and CO₂ molecules on the metal-organic framework MOF-5: ONIOM calculations

Atchara Pianwanit, Chinapong Kritayakornupong, Arthit Vongachariya,
Nattaya Selphusit, **Tanawut Ploymeerusmee**, Tawun Remsungnen, Duangamol
Nuntasri, Siegfried Fritzsche and Supot Hannongbua

Chemical Physics 349 (2008) 77–82



The optimal binding sites of CH₄ and CO₂ molecules on the metal-organic framework MOF-5: ONIOM calculations

Atchara Pianwanit^a, Chinapong Kritayakornupong^b, Arthit Vongachariya^a,
Nattaya Selphusit^c, Tanawut Ploymeerusmee^c, Tawun Remsungnen^d, Duangamol Nuntasri^a,
Siegfried Fritzsche^c, Supot Hannongbua^{a,*}

^a Department of Chemistry, Faculty of Science, Chulalongkorn University, Bangkok 10330, Thailand

^b Department of Chemistry, Faculty of Science, King Mongkut's University of Technology Thonburi, Bangkok 10140, Thailand

^c Petrochemical and Polymer Science Program, Faculty of Science, Chulalongkorn University, Bangkok 10330, Thailand

^d Department of Mathematics, Faculty of Science, Khon Kaen University, Khon Kaen 40002, Thailand

^e Institute for Theoretical Physics, University Leipzig, Postfach 100920, D-04009, Leipzig, Germany

Received 10 October 2007; accepted 20 February 2008

Available online 26 February 2008

Abstract

Optimal binding sites and its corresponding binding energies between MOF-5 clusters and small guest molecules, CH₄ and CO₂, were investigated using the ONIOM method with different levels of quantum chemical calculations. The clusters were validated using three different sizes of the MOF-5 clusters, SINGLE, DOUBLE and TRIPLE consisting of (Zn₄O)₂(COOCH₃)₁₀(COO)₂C₆H₄, (Zn₄O)₃(COOCH₃)₁₄(COO)₄C₆H₄₂ and (Zn₄O)₄(COOCH₃)₁₈(COO)₆(C₆H₄)₃ units, respectively. Guest molecules were assigned to lie in the configurations parallel (||) and perpendicular (⊥) to linker (LINK) and corner (CORN) domains of the clusters. The ONIOM(MP2/6-31G**::HF/6-31G**) with the corrections due to the basis set superposition errors was found to be the optimal choice for the investigation of these systems. Strong effects of cluster size were found for the CO₂/MOF-5 complexes, i.e., the SINGLE cluster is sufficient to represent interactions with CH₄, but the interaction with CO₂ requires the TRIPLE model. The optimal binding sites of guest molecules as well as their orientations in the cavity of the MOF-5 are CORN⊥ for both CH₄ and CO₂ with the corresponding binding energies of −3.64 and −9.27 kJ/mol, respectively.

© 2008 Elsevier B.V. All rights reserved.

Keywords: Metal-organic frameworks; MOF-5; Quantum calculations; ONIOM; Methane; Carbon dioxide

1. Introduction

Metal-organic frameworks (MOFs) are a new class of porous materials which becomes a promising target for gas adsorption, storage and separation [1–3]. Attempts to use alternative fuels such as hydrogen and methane instead of the conventional fuels such as gasoline and diesel have raised the studies of storage applications for such MOFs [4]. Moreover, MOFs have been utilized for separation

and purification of gas mixtures (H₂/CO₂/CH₄). Yaghi and his group introduced the first stable crystal structure of the MOF-5 and generated series of the iso-reticular metal-organic frameworks (IRMOFs) [5–8]. The structure of the IRMOFs composes of basic zinc acetate unit (Zn₄O(CO₂)₆) and linking units (LINK) which are rigid linear dicarboxylate groups. Both units are strongly bonded providing a well-defined structure in which different linking units are possible. In view of an advantage of the modification of such linking units, the MOFs are considered to be the most powerful targets for new storage media in the near future. The understanding of guest–host interactions as well as related properties at molecular level is the key of

* Corresponding author. Tel./fax: +66 2218 7603.

E-mail address: Supot.H@Chula.ac.th (S. Hannongbua).

success to design and discover new class of materials and becomes the main goal of this study.

Some attempts have been made using quantum chemical calculations to study H_2 -MOF-5 interaction. Sagara et al. [9,10] calculated the binding energy based on the second-order Møller–Plesset perturbation theory (MP2) with some models of linker and corner sites. The results show that the binding energy at the corner site (~ 6 – 7 kJ/mol) is a little bit stronger than once at the linker site (~ 4 – 5 kJ/mol). In addition, the investigation of Lee et al. [11] using density functional theory (DFT) shows that the interaction between the simple benzene ring with H_2 is significantly changed when the benzene ring has been incorporated into the framework of MOF-5. Moreover, molecular dynamics simulations have been performed for predicting the adsorption sites of the H_2 [12,13] on the MOF-5 structure. The results again, indicate that hydrogen adsorbs rather strongly at the sites near the zinc acetate cluster and less strongly at the sites near the 1,4-benzenedicarboxylate linker. Yang and Zhong [14] also found that the selectivity of gas absorption is almost pressure-independent. These above results clearly show that the calculated results depend significantly on method and model employed.

To our knowledge, no experimental results are available on the position of preferential CH_4 and CO_2 sites, only neutron spectroscopic techniques proposes at least two different adsorption sites with considerably strong interaction [1]. In this study, different levels of the ONIOM method were applied to investigate the interaction between MOF-5 and small guest molecules, CH_4 and CO_2 , aimed to understand their preferential binding site in the cavity of the MOF-5. The investigations were also extended to seek

for the optimal method used, optimal cluster size of the MOF and the effect of the unbalance of the basis set.

2. Computational details

2.1. Initial structure of the MOF-5

A column consisting of two corners connected by a linker, $(Zn_4O)_2(COOCH_3)_{10}(COO)_2C_6H_4$, was generated (Fig. 1a). It was, then, used to build up the whole MOF-5 unit cell (Fig. 1b). Aimed to get reliable geometries of the MOF-5 relative to experimental data [5], the two fragments were fully optimized using various quantum mechanical methods (semi-empirical, HF, DFT) and basis sets. All optimization and energy calculation were performed using Gaussian03 [15].

2.2. The models

Seeking for an optimal compromise between fragment size vs. the required computer time, different quantum mechanical methods and fragment sizes were examined. The MOF-5 was represented by the three models shown in Fig. 2a. The fragments consisting of 1, 2 and 3 columns were named, for simplicity, as SINGLE, DOUBLE and TRIPLE, respectively.

For interaction with the linker (LINK), guest molecules were generated to move along the vector perpendicular to the molecular plane of the benzene ring at the C_g (see Fig. 1a for definition). For the DOUBLE and TRIPLE models, calculations were carried out only for one wing of the fragments. Here, two possible orientations of guest

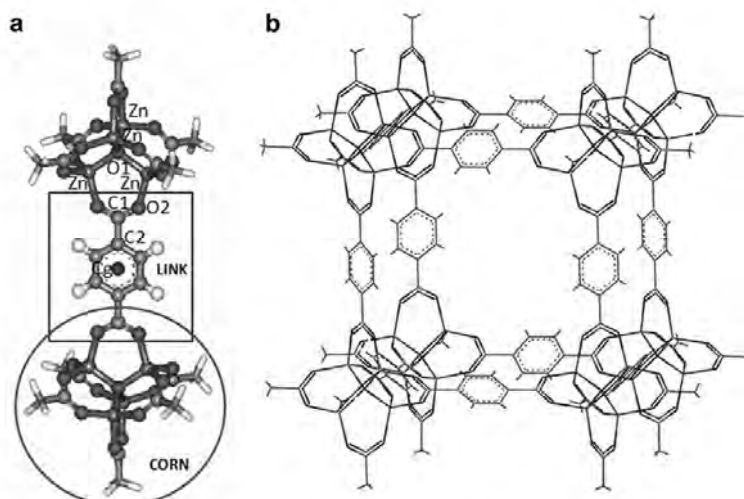


Fig. 1. (a) A single fragment of the MOF-5 consisting of two corners and one linker and (b) the whole MOF-5 unit cell which were generated as initial structures to be used in this study where C_g denotes center of mass of the benzene ring.

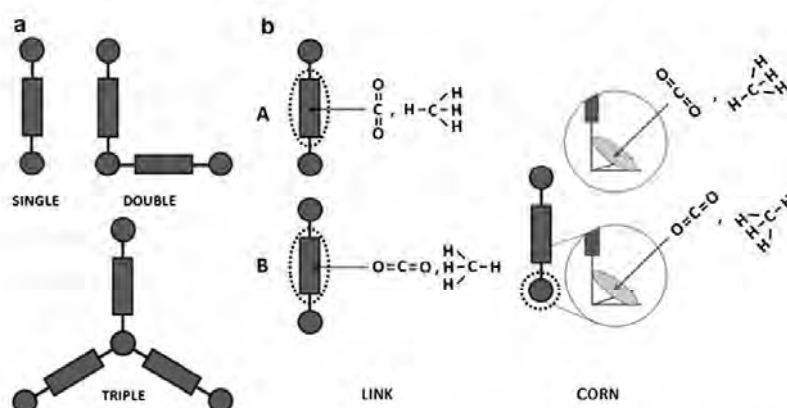


Fig. 2. Representation of the calculated models where rectangular and filled-circle represent linker and corner, respectively, and dot-circle denotes the model part for which high level of accuracy in the ONIOM calculation was applied. (a) Models SINGLE, DOUBLE and TRIPLE represent the MOF fragments containing one, two and three units as oriented, respectively, where one unit of the model is composed of two corners connected by a linker (Fig. 1a). (b) Orientation of guest molecules in parallel (A) and perpendicular (B) to the binding site (linker or corner).

molecules were taken into account, parallel (\parallel) and perpendicular (\perp) to the MOF fragments as shown in Fig. 2b. Precisely, \parallel and \perp for CH₄ means that it points one H atom forward and backward the MOF fragment, respectively. For the MOF corner (CORN), guest molecules, also in the two configurations, were generated to move along the vector pointing to O1 (see Fig. 1a). Note that the vector denotes the C₃-symmetry axis of the three O1–Zn bonds of the MOF corner.

2.3. ONIOM calculations including BSSE

Referred to the three SINGLE, DOUBLE and TRIPLE models defined in Section 2.2, the ONIOM interaction energy of each system, ΔE_{ONIOM} , is derived as

$$\Delta E_{\text{ONIOM}} = E_{(\text{real}, \text{low})} + E_{(\text{model}, \text{high})} - E_{(\text{model}, \text{low})}, \quad (1)$$

where $E_{(\text{real}, \text{low})}$ is the total energy of the real system using the low level method, while $E_{(\text{model}, \text{high})}$ and $E_{(\text{model}, \text{low})}$

Table 1

Selected bond distances and bond angles obtained from the geometry optimizations for the two clusters shown in Fig. 1 where the experimental data [5] and the other theoretical calculations [16,17] were also given for comparison (see Fig. 1 for atomic labels)

Method/basis set	Bond length (pm)				Bond angle (°)		
	Zn–O ₁	Zn–O ₂	O ₂ –C ₁	C ₁ –C ₂	O ₁ –Zn–O ₂	Zn–O ₂ –C ₁	O ₂ –C ₁ –C ₂
<i>(a) One column cluster (Fig. 1a)</i>							
AM1	205.5	212.4	128.5	148.5	110.1	134.2	119.0
PM3	195.1	205.3	127.6	150.7	112.4	131.2	118.2
HF/6-31G*	197.8	196.9	124.5	149.7	110.1	132.8	117.7
HF/6-31G**	197.8	196.9	124.5	149.7	110.1	132.8	117.7
B3LYP/6-31G*	195.4	195.0	127.0	149.6	111.2	131.1	117.2
B3LYP/6-31G**	195.3	195.1	127.0	149.6	111.1	131.2	117.2
B3LYP/6-311G**	196.1	195.7	126.4	149.6	109.7	131.1	117.3
B3LYP/6-311G** [16]	197.2	195.3	126.2	151.0	110.8	131.7	117.8
GULP [16]	212.6	195.7	127.2	138.8		134.5	120.3
MPW1PW91/6-31G**	194.0	194.0	126.4	149.1	111.2	131.0	117.2
<i>(b) One unit cell cluster (Fig. 1b)</i>							
AM1	205.4	212.1	128.5	148.5	110.2	134.2	119.0
PM3	195.1	205.4	127.5	150.7	112.1	130.7	117.6
B3LYP/6-31G**	195.3	194.8	127.0	149.6	111.4	131.1	117.3
AM1 [17]	205.5	212.4	128.4	148.5	110.1	134.2	119.0
PM3 [17]	195.1	205.6	127.5	150.7	112.1	130.6	117.5
Experimental data	193.6	194.1	125.2	149.8	111.1	132.3	118.1

denote the total energies of the model part calculated with high and low level methods, respectively. The method used for the high:low levels was represented by MP2/6-31G**: $\text{HF}/6\text{-}31\text{G}^{**}$. The high accurate (model) MP2/6-31G** part covers the compositions (C_6H_4) and the ($\text{Zn}_4\text{O}(\text{CO}_2)_6$) for the linker and corner domains, respectively, labeled as dot-circles in Fig. 2. The real parts were the whole SINGLE, DOUBLE and TRIPLE fragments shown in Fig. 2. Discrepancies due to an unbalance of the basis set used, known as basis set superposition error (BSSE) were examined and taken into account for all data points reported in this study.

3. Results and discussion

3.1. Geometries of the MOF-5

Starting from the two clusters, one column (Fig. 1a) and the whole unit cell (Fig. 1b) of the MOF-5, their intramolecular geometries (bond lengths and bond angles) were fully optimized using different methods and levels of accuracy. The results were summarized in Table 1.

Relative to experimental geometries [5], discrepancies were, as expected, found among the results obtained from different methods and basis sets used. The MPW1PW91/6-31G** geometries for the one column cluster are in excellent agreement with the experimental data. Due to the fact that the MPW1PW91/6-31G** is highly time consuming, it is practically impossible to apply it for the full unit cell cluster. Therefore, the optimal choice shifts to the next lower-accurate B3LYP/6-31G* and B3LYP/6-31G** meth-

ods. As shown in Table 1, no significant difference was found on the geometries of the clusters yielded from these two methods. However, the MP2/6-31G** binding energy is slightly lower than that of MP2/6-31G* (data not shown) although the time required is also slightly longer. Taking into account all the data mentioned earlier, the MP2/6-31G**, with BSSE corrections, was chosen to represent the high accurate part of the ONIOM calculation.

Note that the results yielded from the two clusters, one column and one unit cell, are in good agreement. This indicates that size of the one column cluster is sufficient to represent intramolecular geometries of the MOF-5. In addition, our results, especially Zn–O1 and Zn–O2 distances, are closer to the experimental data [5] in comparison to those reported in Refs. [16,17].

3.2. Effect of an unbalance of the basis sets

Fig. 3 shows the ONIOM binding energies with and without BSSE corrections between CH_4 and the three clusters, SINGLE, DOUBLE and TRIPLE, of the MOF-5 (see Fig. 2a) where CH_4 points one H atom forward Cg or O1 and the distances are from C atom of CH_4 to Cg or O1 (see Fig. 1a) for linker (LINK||) or corner (CORN||) clusters, respectively.

It was surprisingly found from the plots that BSSE leads to dramatic changes of the calculated results. Distance to the minimum changes from 3.74 to 4.08 Å for the SINGLE LINK|| and from 4.19 to 4.92 Å for the SINGLE CORN|| clusters. The corresponding interaction energy differences for the linker and corner are ~ 3 and ~ 9 kJ/mol,

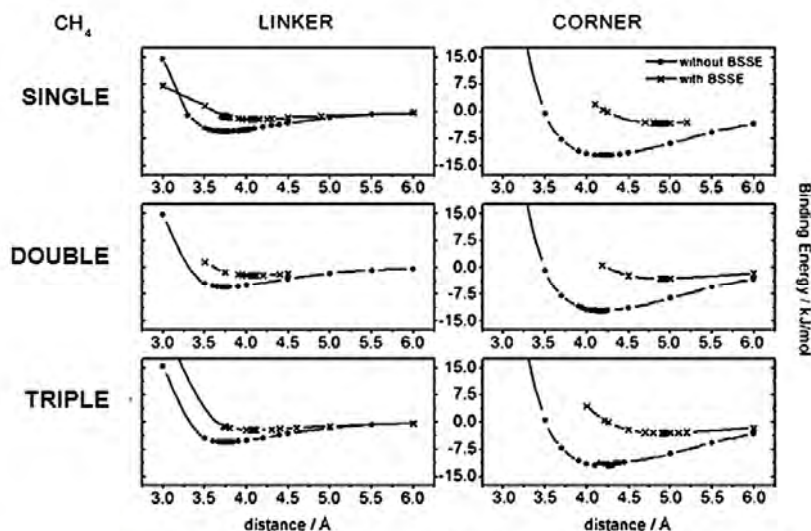


Fig. 3. ONIOM binding energies with and without BSSE corrections for the CH_4 /MOF-5 complexes where CH_4 was located in the configuration pointing one H atom to the MOF-5 (||, see Fig. 2b) and the MOF-5 was represented by the SINGLE, DOUBLE and TRIPLE clusters (see Fig. 2a). For the linker (LINK) and corner (CORN) calculations, the distances were measured from the C atom of CH_4 to Cg and O1, respectively (see Fig. 1a).

respectively, shifted to weaker interactions. The observed results indicate obviously that the investigated systems require BSSE corrections.

3.3. MOF-guest binding

ONIOM binding energy between MOF-5 in the three cluster models, SINGLE, DOUBLE and TRIPLE (Fig. 2a) and guest molecules in the two orientations, \parallel and \perp , (Fig. 2b) were calculated separately for the linker and corner parts and summarized in Table 2. The distances were measured from Cg (for linker) and O1 (for corner) to C atoms of CH₄ and CO₂. The BSSE corrections were applied in all data points.

Considering the binding energies at the same configuration of guest molecules (\parallel or \perp) at the linker part (Table 2a), no significant difference was found for the CH₄ complexes of different cluster sizes, SINGLE, DOUBLE and TRIPLE. However, the cluster size effect was slightly found for the CO₂ complexes, i.e., increasing of the MOF-5 cluster from SINGLE to TRIPLE leads to weaker binding energy (from -5.32 to -5.08 kJ/mol) for the \parallel whereas this change was opposite (from -1.61 to -2.02 kJ/mol) for the \perp configurations. For the effects of molecular orientation, the binding energy of the \parallel configuration for the CO₂/MOF-5 complexes is about three times more stable than that in the \perp configuration but only slightly different for the CH₄ complexes.

In contrast to what was observed for the linker, the calculated results at the MOF-5 corner (Table 2b) lead to the following two main conclusions: (i) CO₂ prefers to approach O1 (defined in Fig. 1b) at the corner of the MOF-5 in the \perp configuration, i.e., the binding energies

of the \parallel configuration of -4.94 , -3.55 and -2.25 kJ/mol are obviously less stable than those of the \perp configuration of -6.72 , -8.14 and -9.27 kJ/mol, respectively. A similar trend was, somehow, found for the CH₄ binding in which the interaction energy in the configuration where CH₄ points one H backward O1 is slightly lower than that when one H points forward O1. (ii) Effects of cluster size were found to be strong for the CO₂/MOF-5 complexes. As shown, an increasing of the cluster size from SINGLE to TRIPLE decreases the binding energy of the \parallel configuration from -4.94 to -2.25 kJ/mol. In contrast, this change leads to an increasing of the binding energy of the \perp configuration from -6.72 to -9.27 kJ/mol. The detected data let us conclude that for guest molecules of similar or bigger size than CO₂, the minimum cluster size to represent the MOF corner must contain at least three SINGLE MOF units (see Fig. 2a).

Taking into account all the data discussed above for both CH₄ and CO₂ molecules, interactions at the MOF's corner are stronger than those at the linker. This can be due to the fact that the interaction with the arene ring (see Fig. 1) of the linker unit is dominated by the dispersion forces. This is not the case for the MOF's corner where the interaction is influenced by electronic forces due to the (Zn₄O)₂(COOCH₃)₁₀ unit.

Note that the results show a certainly relevant trend of the interaction energies with CH₄ and CO₂ guest molecules. However, a higher level of quantum treatment is needed in order to provide an absolute value of the binding energies.

In summary, the optimal binding sites of guest molecules as well as their orientations in the cavity of the MOF-5 based on the binding energies shown in Table 2 are CORN \perp for both CH₄ and CO₂ complexes. In addition, the binding energies of the MOF-5 with the two guest molecules complexes are in the following order: CH₄: CORN \perp < CORN \parallel < LINK \parallel < LINK \perp and CO₂: CORN \perp < LINK \parallel < CORN \parallel < LINK \perp .

4. Conclusion

Quantum chemical calculations were carried out to find the optimal binding site and orientation as well as the binding energy of CH₄ and CO₂ molecules in the cavity of MOF-5. Guest molecules were assigned to lie in the configurations parallel (\parallel) and perpendicular (\perp) to linker (LINK) and corner (CORN) domains. The ONIOM (MP2/6-31G**:*HF*/6-31G**) method was found to be a compromise between the accuracy and computer time required for the investigated system. Unbalance of the basis set used, known as basis set superposition errors, was found to effect the calculated results, both binding distance and energy, significantly. The cluster size of (Zn₄O)₂(COOCH₃)₁₀(COO)₂C₆H₄ is sufficient to represent interactions at both linker and corner domains of the MOF-5 with CH₄ molecules. However, for guest molecules of similar or bigger size than CO₂, the minimum cluster size to represent the MOF corner must contain at least one

Table 2
ONIOM binding energies with BSSE corrections and the corresponding distances between MOF-5 in the three cluster models (SINGLE, DOUBLE and TRIPLE in Fig. 2a) and guest molecules in the two orientations (\parallel and \perp in Fig. 2b) in which the distances were measured from Cg (for linker) and O1 (for corner) to C atoms of CH₄ and CO₂.

Model	MOF-5	Guest	Distance Cg–C (Å)		Binding energy (kJ/mol)	
			CH ₄	CO ₂	CH ₄	CO ₂
<i>(a) At the MOF-5 linker</i>						
SINGLE	\parallel	\perp	4.08	3.59	-2.15	-5.32
			3.97	4.64	-1.86	-1.61
DOUBLE	\parallel	\perp	4.09	3.58	-2.17	-5.16
			3.98	4.65	-1.84	-1.84
TRIPLE	\parallel	\perp	4.10	3.59	-2.15	-5.08
			3.98	4.66	-1.83	-2.02
Model	MOF-5	Guest	Distance O1–C (Å)		Binding energy (kJ/mol)	
<i>(b) At the MOF-5 corner</i>						
SINGLE	\parallel	\perp	4.92	5.03	-3.18	-4.94
			4.90	5.06	-3.64	-6.72
DOUBLE	\parallel	\perp	4.90	5.01	-3.11	-3.55
			4.91	5.04	-3.74	-8.14
TRIPLE	\parallel	\perp	4.92	5.04	-3.00	-2.25
			4.90	5.03	-3.80	-9.27

corner of $(\text{Zn}_4\text{O})(\text{CO}_2)_6$ and three edges of $((\text{Zn}_4\text{O})(\text{CO}_2)_6(\text{C}_6\text{H}_4)_3)$ unit in perpendicular. The optimal binding sites for the CH_4 and CO_2 molecules are at the corner. CH_4 was found to point one H atom backward and along the C_3 -symmetry axis of the corner of the MOF unit cell. For CO_2 , it prefers to approach the MOF corner by moving the C atom along the C_3 axis and its molecular axis is perpendicular to the C_3 axis. The optimal binding energies for CH_4 and CO_2 are -3.64 and -9.27 kJ/mol, respectively.

Acknowledgements

The authors would like to thank the Postdoctoral Fellowship granting by the Commission on Higher Education (CHE), the Thailand research fund (TRF) and the Deutsche Forschungsgemeinschaft (DFG Project 1486/1-4) for the financial support. The Computational Chemistry Unit Cell at Department of Chemistry, Faculty of Science, Chulalongkorn University and the Scientific Mathematics Advanced Research Tasks at Department of Mathematics, Faculty of Science, Khon Kaen University, are acknowledged for all computer resources and other facilities.

References

- [1] N.L. Rosi, J. Eckert, M. Eddaoudi, D.T. Vodak, J. Kim, M. O'Keeffe, O.M. Yaghi, *Science* 300 (2003) 1127.
- [2] J.L.C. Rowsell, A.R. Millward, K.S. Park, O.M. Yaghi, *J. Am. Chem. Soc.* 126 (2004) 5666.
- [3] J.L.C. Rowsell, E.C. Spencer, J. Eckert, J.A.K. Howard, O.M. Yaghi, *Science* 309 (2005) 1350.
- [4] J.L.C. Rowsell, O.M. Yaghi, *J. Am. Chem. Soc.* 128 (2006) 1304.
- [5] H. Lir, M. Eddaoudi, M. O'Keeffe, O.M. Yaghi, *Nature* 402 (1999) 276.
- [6] M. Eddaoudi, J. Kim, N. Rosi, D. Vodak, J. Wachter, M. O'Keeffe, O.M. Yaghi, *Science* 295 (2002) 469.
- [7] O.M. Yaghi, M. O'Keeffe, N.W. Ockwig, H.K. Chae, M. Eddaoudi, J. Kim, *Nature* 423 (2003) 705.
- [8] J.L.C. Rowsell, O.M. Yaghi, *Microporous Mesoporous Mater.* 73 (2004) 3.
- [9] T. Sagara, J. Klassen, E. Ganz, *J. Chem. Phys.* 121 (2004) 1254.
- [10] T. Sagara, J. Klassen, J. Ortony, E. Ganz, *J. Chem. Phys.* 123 (2005) 14701.
- [11] T.B. Lee, D. Kim, D.H. Jung, S.B. Choi, J.H. Yoon, J. Kim, K. Choi, S.-H. Choi, *Catal. Today* 120 (2007) 330.
- [12] Q. Yang, C. Zhong, *J. Phys. Chem. B (Lett.)* 109 (2005) 11862.
- [13] T. Mueller, G. Ceder, *J. Phys. Chem. B* 109 (2005) 17974.
- [14] Q. Yang, C. Zhong, *J. Phys. Chem. B* 110 (2006) 17776.
- [15] M.J. Frisch, G.W. Trucks, H.B. Schlegel, G.E. Scuseria, M.A. Robb, J.R. Cheeseman, J.A. Montgomery, T. Vreven, K.N. Kudin, J.C. Burant, J.M. Millam, S.S. Iyengar, J. Tomasi, V. Barone, B. Mennucci, M. Cossi, G. Scalmani, N. Rega, G.A. Petersson, H. Nakatsuji, M. Hada, M. Ehara, K. Toyota, R. Fukuda, J. Hasegawa, M. Ishida, T. Nakajima, Y. Honda, O. Kitao, H. Nakai, M.L. Klene, X. Li, J.E. Knox, H.P. Hratchian, J.B. Cross, V. Bakken, C. Adamo, J. Jaramillo, R. Gomperts, R.E. Stratmann, O. Yazyev, A.J. Austin, R. Cammi, C. Pomelli, J.W. Ochterski, P.Y. Ayala, K. Morokuma, G.A. Voth, P. Salvador, J.J. Dannenberg, V.G. Zakrzewski, S. Dapprich, A.D. Daniels, M.C. Strain, O. Farkas, D.K. Malick, A.D. Rabuck, K. Raghavachari, J.B. Foresman, J.V. Ortiz, Q. Cui, A.G. Baboul, S. Clifford, J. Cioslowski, B.B. Stefanov, G. Liu, A. Liashenko, P. Piskorz, I. Komaromi, R.L. Martin, D.J. Fox, T. Keith, M.A. Al-Laham, C.Y. Peng, A. Nanayakkara, M. Challacombe, P.M.W. Gill, B. Johnson, W. Chen, M.W. Wong, C. Gonzalez, J.A. Pople, Gaussian03, Revision C.02, Gaussian, Inc., Wallingford CT, 2004.
- [16] B.L. Huang, A.J.H. McGaughey, M. Kaviani, *Int. J. Heat Mass Transfer* 50 (2007) 393.
- [17] C.F. Braga, R.L. Longo, *J. Mol. Struct. (Theochem.)* 716 (2005) 33.

Appendix B:**MANUSCRIPT****Metal organic frameworks as carbon dioxide storage studied by
molecular dynamic simulations**

**Tanawut Ploymeerusmee, Oraphan Saengsawang, Duangamol Nuntasri, Tawun Remsungnen, Siegfried
Fritzsche, Supot Hannongbua**

To be submitted

Metal organic frameworks as carbon dioxide storage studied by molecular dynamic simulations

Tanawut Ploymeerusmee¹, Oraphan Saengsawang², Duangamol Nuntasri³, Tawun Remsungnen⁴, Siegfried Fritzsche⁵, Supot Hannongbua^{2,*}

¹*Petrochemical and Polymer Science Program, Faculty of Science, Chulalongkorn University, Bangkok 10330, Thailand*

²*Computational Chemistry Unit cell (CCUC), Department of Chemistry, Faculty of Science, Chulalongkorn University, Bangkok 10330, Thailand*

³*Department of Chemistry, Faculty of Science, Chulalongkorn University, Bangkok 10330, Thailand*

⁴*Department of Mathematics, Khon Khaen University, Khon Khaen, Thailand*

⁵*Institut für Theoretische Physik, Universität Leipzig, Vor dem Hospitaltore 1, D-04103, Leipzig, Germany*

Abstract

The excess emission of carbon dioxide (CO₂), *e.g.*, releasing from manufactory and power plant generator is the major cause of global warming. Metal-Organic Frameworks (MOFs) become a primary target for CO₂ storage production. MOFs consist of zinc oxo acetate clusters and various aromatic organic linkers providing a series of Isorecticular MOFs (IRMOFs). Molecular dynamic simulations of 2×2×2 lattice units of MOF-5 with the loading of 8, 64, 128, 256, 512 molecules of CO₂ per simulation cube (MPC) were performed at 300 K. The obtained results are in agreement with those found previously from ONIOM calculations that CO₂ prefers to absorb at the MOF-5 corner site. Interestingly, conclusion at MPC=512, the CO₂ was found to form second layer coordinated weakly to fill the rest space around the MOF-5 corner. The average coordination numbers of CO₂ at the corner and the linker sites are 2.9 and 3.1 molecules, respectively.

Keywords: gas storage, carbon dioxide, MOF-5, MD simulation, binding site.

To whom correspondence should be sent

Email address: supot.h@chula.ac.th (Supot Hannongbua)

1. Introduction

Natural fuel such as coal, petroleum oils and natural gases are mainly used by human in many activities, e.g., transportation, industry and electric power station. These lead not only gain desired products, heat, energy and electricity, but also undesired ones, greenhouse gas such as carbon dioxide (CO_2) *etc.* Amount of CO_2 released to atmosphere causes serious environment problem, consequently, global warming. Gas storage application is initiated and continuously developed to reduce amount of undesired gas like CO_2 in atmosphere. The materials which have high surface areas and stability are required to construct the best storage.

Metal-organic frameworks (MOFs) were firstly discovered by Yaghi *et al.* (1) and become a promising target for gas storage, separation and catalysis application (1-6). The MOF-5 is one candidate in series of the iso-reticular metal-organic frameworks (IRMOFs). The unit cell of MOF-5 consists of zinc oxide cluster linked with dicarboxylate group in three-dimensional cubic framework providing a crystalline structure as shown in Figure 1. Both oxide cluster and linker can be modified by synthesis with different organic linkage and metal oxide, respectively. Resulting in a structure was demonstrated that it has higher surface area and pore volume than most porous crystalline material.

The basic understanding of gas behavior inside MOF such as the adsorption site and preferential gas orientation is one of the key factor to improve and develop gas storage technology. The obtained basic information is expected to be the guideline for designation of the new material with high capability in gas storage application. In this study the molecular dynamic (MD) simulation were perform to CO_2 -MOF-5 system. The loading of CO_2 molecule inside the MOF-5 lattice was varied in order to study the preferred adsorption site and gas behavior. Moreover, the obtained results were compared to the one yielded from ONOIM calculation, previously.

2. Calculation details

2.1 Initial lattice structure

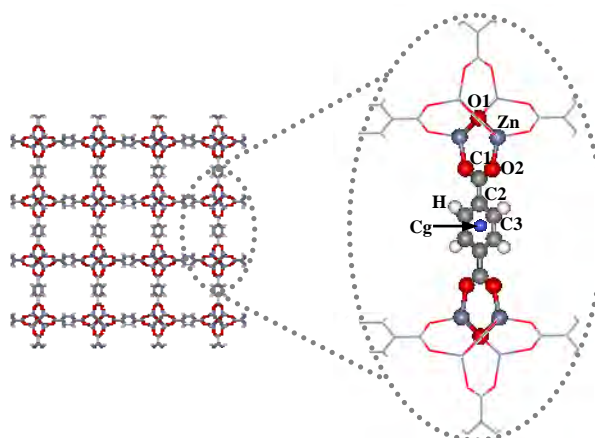


Figure 1. The $2 \times 2 \times 2$ unit cells of simulation lattice used and atom type in the MOF-5. Cg is an average of the coordinates of the 6 carbon atoms of the benzene ring.

The initial atomic coordinates of MOF-5 used in molecular dynamic simulation were taken from x-ray crystal structure (7), which has a cubic unit cell with $Fm3m$ space group and lattice length of 25.8 Å. It was, then, used as prototype to build up 8 unit cells of MOF-5 in $2 \times 2 \times 2$ grid. The obtained simulation cube contains 3,392 atoms with the lattice length of 51.78 Å.

2.2 Force field parameters

Carbon dioxide and MOF-5 were represented as rigid models, in which the intermolecular interaction between MOF-5 and CO_2 was calculated using Coulomb and Lennard-Jones pair potential. The LJ potential parameters for carbon dioxide were taken from the EPM model force field developed by Harris and Yung (8). The MOF-5 structure contains 8 atom types were labeled in Figure 1. Potential parameters for non-bonded interaction of MOF-5 were taken from Greathouse *et al.* (7)

2.3 Molecular dynamic simulations

With 8 unit cells of MOF-5 as described in section 2.1, the simulations were carried out at 8, 64, 128, 256 and 512 molecules of CO_2 per simulation cubic (MPC). Periodical boundary condition is applied to avoid finite size effect. The simulations were performed with NVT ensemble which is suitable for rigid system (7). The time step was

0.05 fs and the production part of 1 ns was achieved after the equilibration period of 1 ps. The average temperature of the system is 300 K. All simulations were performed with DL_POLY 2 package (9).

3. Results and discussion

3.1 Structure of CO₂ at the MOF-5 corner

To monitor structural data of CO₂ in MOF-5, atom-atom radial distribution functions (RDF), expressed as $g_{ij}(r)$, the probability of finding a particle of type j in a sphere of radius, r , around a particle of type i , were calculated. The MOF-CO₂ RDFs were evaluated separately for those where i denotes O1 of MOF-5 and middle of the benzene ring of the MOF-5 linker (Cg that generated as an average of the coordinates of the 6 carbon atoms of the benzene ring) and j is C and O atoms of CO₂ (see Figure 1 for atomic labels). The corresponding O1-C, O1-O, Cg-C and Cg-O RDFs were given in Figures 2 and 3. In addition, distribution of the corresponding coordination number calculated up to the first minimum of the O1-O and the Cg-O RDFs were also examined and plotted in Figures 2c and 3c, respectively.

Characteristics of CO₂ adsorption at the MOF-5 corner can be understood from the O1-C and O1-O RDFs (Figures 2a and 2b). The plots for all concentrations of the O1-C and O1-O RDFs show a first sharp peak centered at 4.70 Å and 3.82 Å, respectively. This indicates that CO₂ adsorbs firmly to the MOF-5 corner in which the average distances from O1 of MOF-5 (see Figure 1 for definition) to C and O atoms of CO₂ are 4.70 Å and 3.82 Å, respectively. The two peaks of the O1-O RDFs centered at 3.82 Å and 5.70 Å denote the distances from O1 to the two oxygen atoms of CO₂ whereas the distance between the two maxima of 1.88 Å is almost the same as that of the length of the CO₂ molecule (2.32 Å). This feature suggests us to preliminary conclude that CO₂ points, somehow, its molecular axis to the MOF-5 corner, O1 atoms. Precise orientations of the CO₂ was calculated and discussed again in section 3.3. Interest is focused to the O1-C RDF for the loading of 256 MPC shown in Figure 2b where the RDF shoulder at ~5.6 Å starts to be detected. This shoulder is more pronounced at 512 MPC whereas position of the first peak remains unchanged, compared to the other concentrations. This indicates a structural formation of the CO₂ in the MOF-5 cavity. More details investigations and discussions were given in the next section.

To examine number of CO₂ molecules coordinated to the MOF-5 corner, the results were displayed in Figure 2c in terms of their distributions, evaluated up to the first minimum of 4.90 Å of the O1-O RDFs of the five concentrations. The plots represent number of the first O atom of CO₂ molecules lying under the first peak centered at 3.82 Å of the O1-O RDF (Figure 2a). Broad distribution of the coordination numbers shown in Figure 2c as well as non-zero of the peak height at the first minimum of the O1-O RDF indicates weak interactions of CO₂ at the MOF-5 corner and mobility of the coordinated CO₂ molecules lying under the first two peaks of the O1-O RDF, respectively. As expected, the average coordination number was observed to increase as a function of loading, from 0.07 to 0.6, 1.2, 2.2 and 2.9 CO₂ molecules when the loading increases from 8 to 64, 128, 256 and 512 MPC.

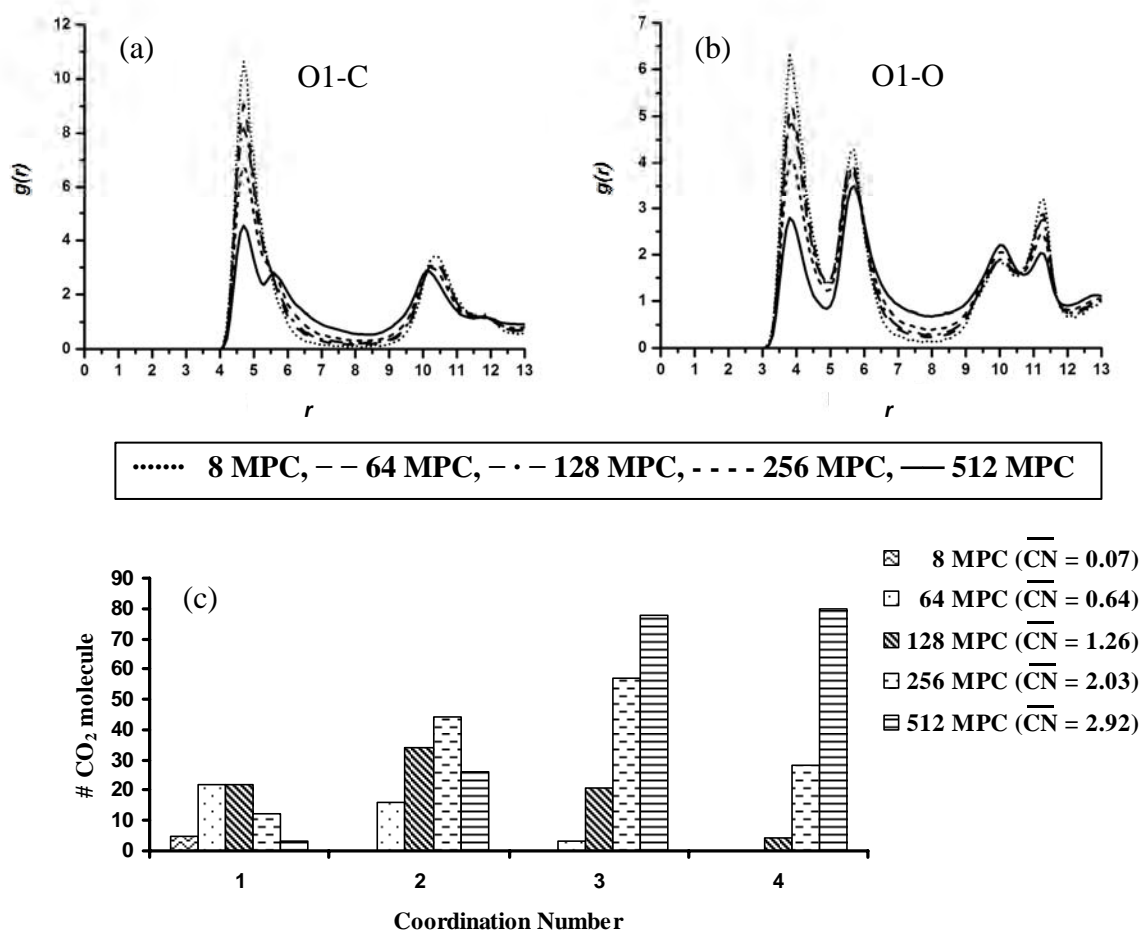


Figure 2. (a)-(b) RDFs for the 5 loadings of CO₂, centered at O1 of MOF-5 (see Figure 1 for atomic labels) to O and C atoms of CO₂, respectively. (c) Distribution of the

corresponding coordination number calculated up to the first minimum of 4.90 Å of the O1-O RDF where the average coordination numbers (\overline{CN}) were also shown.

3.2 Structure of CO₂ at the MOF-5 linker

As defined above, the Cg-C and Cg-O RDFs representing the distribution of C and O atoms of CO₂ around the Cg (center of the benzene ring) of the MOF-5 linker were calculated and plotted in Figures 3a and 3b, respectively. Here, distribution of the corresponding coordination number calculated up to the first minimum of 6.00 Å of the Cg-O RDF (Figure 3a) were shown in Figure 3c.

The Cg-C and Cg-O RDFs for all concentrations show sharp first peak at 4.76 Å and 5.25 Å, respectively. An appearing of the two maxima of the two RDFs at almost the same distance indicates free orientation of the CO₂ coordinated to the MOF-5 linker. This conclusion was also supported by an emerge of single Cg-O peak due to the two oxygen atoms of CO₂ molecule. Because of such weakly binding, not much structural data can be extracted from these RDFs.

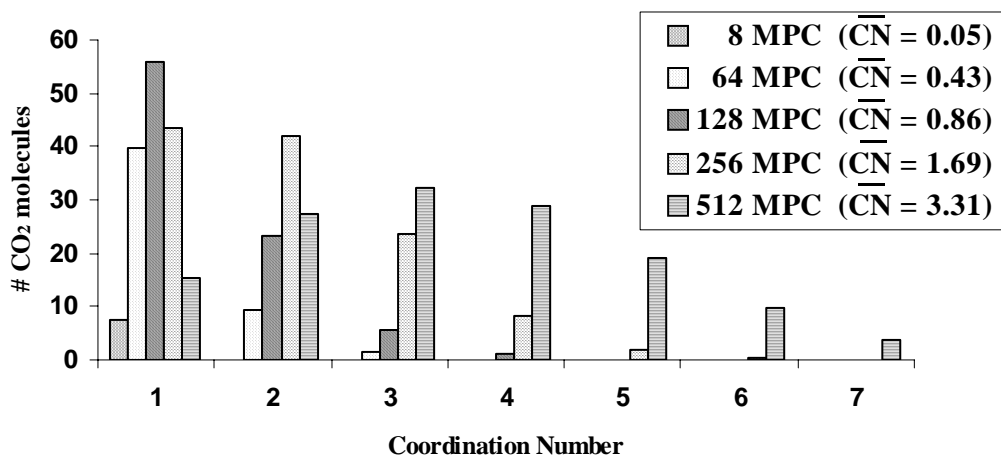
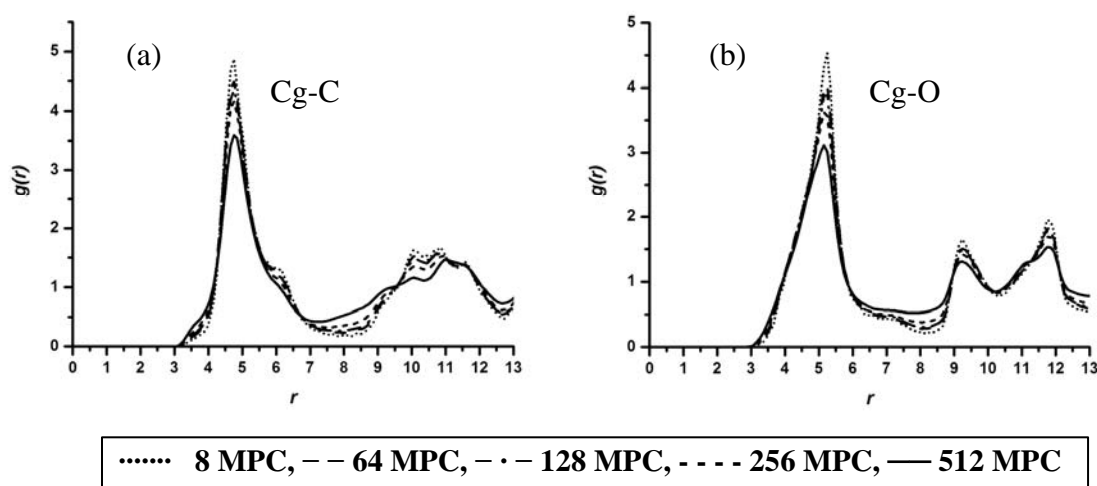


Figure 3. (a)-(b) RDFs for the 5 loadings of CO₂, centered at the middle of benzene ring of the MOF-5 linker, Cg (see text for definition), to O and C atoms of CO₂, respectively. (c) Distribution of the corresponding coordination number averaged up to the first minimum of 6.00 Å of the Cg-O RDF where the average coordination numbers (\overline{CN}) were also shown.

3.3 Orientation of CO₂ around the MOF-5 binding site

To visualize orientation of CO₂ which coordinate to the corner and the linker binding sites, distribution of the angle θ , defined by the three atoms O1-O-C, was evaluated. Here, O1 still denote the MOF-5 atom (Figure 1) while O and C are the two atoms of CO₂. The plots for all concentrations were given in Figure 4a for the CO₂ lying under first peak of the O1-O RDF ($0.0 \text{ \AA} \leq r \leq 4.90 \text{ \AA}$). For the loading of 512 MPC, the results were also plotted separately (an inset of the Figure) for the CO₂ located under the first peak ($0.0 \text{ \AA} \leq r \leq 5.20 \text{ \AA}$) and the second peak ($5.20 \text{ \AA} < r \leq 6.50 \text{ \AA}$) of the O1-C RDF (maximum and minimum limits of r were assigned regarding the minima of the focused peaks shown in Figure 2). In addition, the same plots were given in Figure 4b for the CO₂ coordinated to the MOF-5 linker (locate under the first peak of the Cg-O RDF at $0.0 \text{ \AA} \leq r \leq 6.00 \text{ \AA}$) where the angle ϕ was defined by the Cg-O-C atoms.

Exclude the loading of 512 MPC, the distribution plots for all concentrations of the MOF-5 corner representing orientation of the CO₂ lying within the first peaks of the O1-O RDF show two maxima at $\theta = \sim 35^\circ$ and $\sim 130^\circ$. This indicates orientation of the nearest neighbors of O1, and hence the MOF-5 corner, in the manner to tilt their molecular axis by 35° to 50° ($180^\circ - 130^\circ$ due to the second peak) from the O1-C axis (see also an inset of Figure). Interest is focused to the distribution plots for the 512 MPC as shown in an inset. This is in connection with the change of the structural property in which the RDF for the 512 MPC loading was found to form pronounced shoulder at $\sim 5.6 \text{ \AA}$ (Figure 2a). Whereas the two pronounced peaks at $\theta = \sim 35^\circ$ and $\sim 130^\circ$ (solid line of an inset) which are the characteristic of the nearest neighbors remain unchanged, the other peak at $\sim 90^\circ$ (dot line in an inset) was additional yielded. The newly detected peak indicates the formation of another layer of CO₂ (located under the shoulder of the O1-C RDF) which aligns their molecular axis perpendicular to the O1-C axis. The observed data suggest us to conclude that the CO₂ lying in this layer behave as the first shell

coordination numbers of the CO₂ located under the O1-C RDF first peak. Simultaneously, they are also proposed to coordinate weakly to fill in the rest space around the MOF-5 corner. Note that the distance of ~ 0.9 Å from the first peak (at 4.70 Å) to its shoulder (at ~ 5.6 Å) of the O1-C RDF (Figure 2a) is too short to claim that this layer of CO₂ is the second coordination shell of O1.

For the MOF-5 linker, the plots for all concentrations show broad distribution ranging from 0° to 180° with the maxima at $\phi = \sim 80^\circ$ (Figure 4b). This indicates a free orientation of the CO₂ molecules which coordinate to the MOF-5 linker. Although the favorite alignment is to point their molecular axis perpendicular to the Cg-O axis (an inset of Figure)

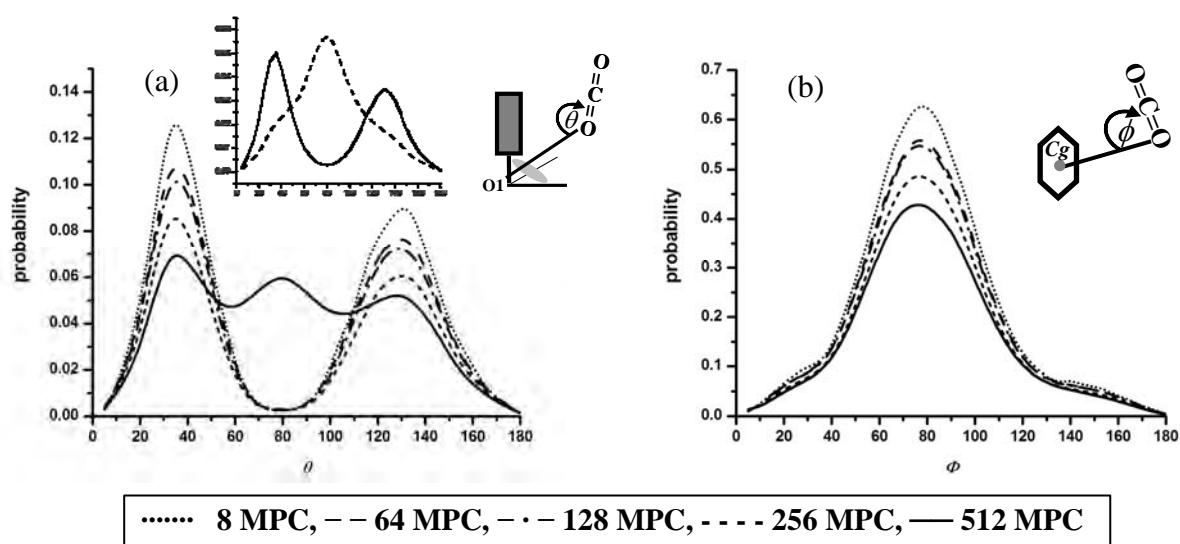


Figure 4. Distribution of the angles θ and ϕ representing orientation of CO₂ lying under the first peak of the O1-O RDF (a) and the Cg-O RDF (b) where the plots for the 2 peaks of the O1-C RDF at the loading of 512 MPC was given separately in an inset (see text for more details).

3.4 CO₂-CO₂ radial distribution functions

Figures 5a and 5b, the RDFs centered at C atom of one CO₂ to C and O atoms of the other CO₂ were monitored and represented as C-C and C-O, respectively. As can be clearly seen, no significant difference was found in terms of the peak position. The C-C RDFs for all concentrations show sharp first peak at 4.13 Å indicating structural formation of CO₂ clusters in the MOF-5 cavity. Due to a weak interaction between the

CO₂ molecules, therefore, preferential orientation can not be formed, and hence, no sharp peaks were found for the C-O RDF. In addition, the average coordination numbers of CO₂ for the loadings of 8 to 64, 128, 256 and 512 MPCs calculated up to the first minimum of 5.50 Å of the C-C RDF are 1.02, 1.14, 1.27, 1.67 and 2.76 molecules, respectively.

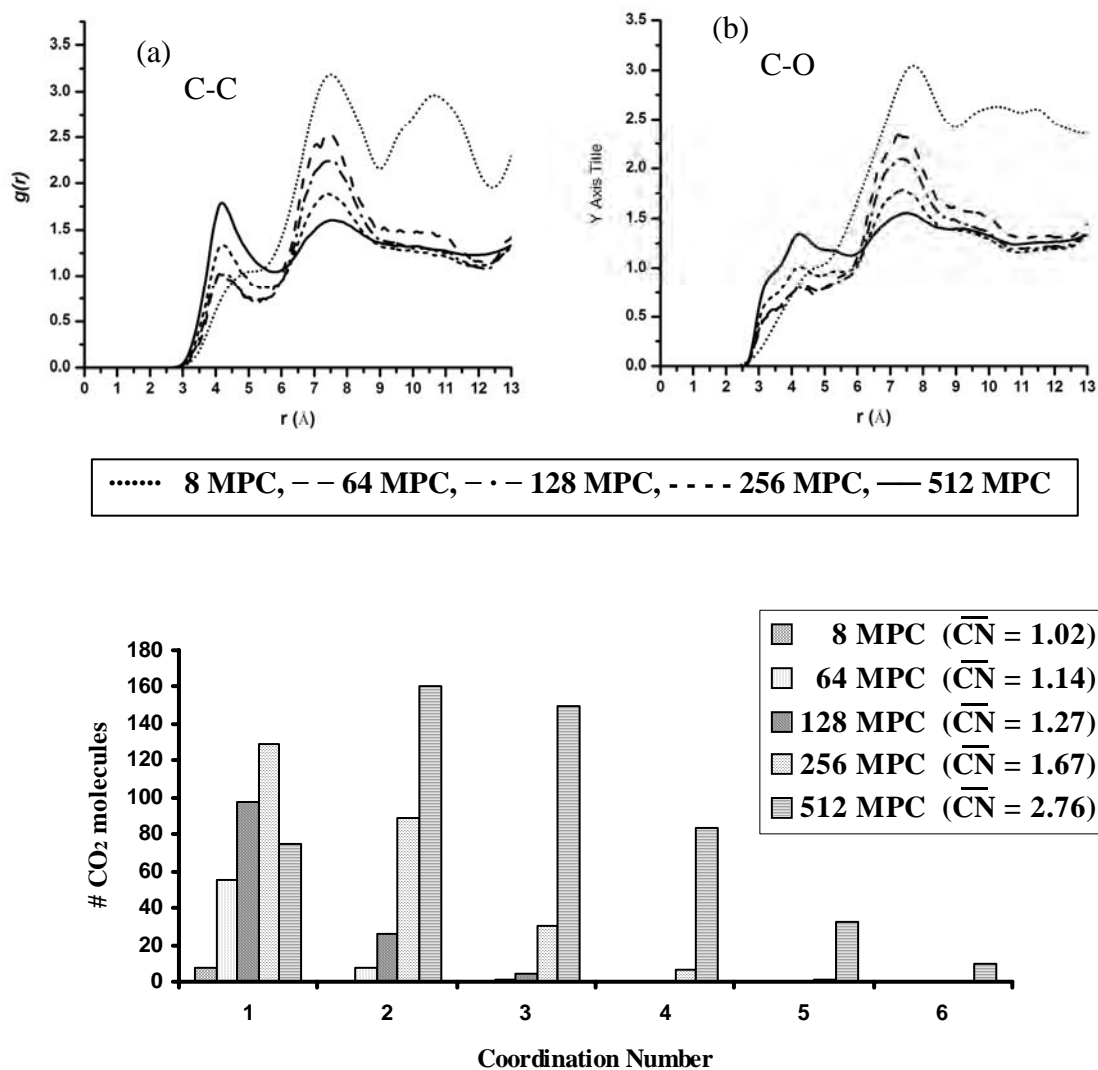


Figure 5. (a)-(b) C-C and C-O Radial distribution functions (RDF) for the 5 loadings of CO₂. (c) Distribution of the corresponding coordination number averaged up to the first minimum of 5.50 Å of the C-C RDF where the average coordination numbers (\overline{CN}) were also shown.

4. Conclusion

Molecular dynamic simulations of $2 \times 2 \times 2$ lattice units of MOF-5 with the loading of 8, 64, 128, 256 and 512 molecules of CO_2 per simulation cube (MPC) were performed at 300 K. The obtained results are in agreement with those found from ONIOM calculations in ref. [xx] that CO_2 prefers to absorb at the MOF-5 corner site. To visualize orientation of CO_2 which coordinate to the corner and the linker binding sites, distribution of the angle θ , defined by the three atoms O1-O-C, was evaluated, where O1 denotes oxygen atom at the MOF corner, O and C are the two atoms of CO_2 . Exclude the loading of 512 MPC, the distribution plots for all concentrations of the MOF-5 corner take place at $\theta = \sim 35^\circ$ and $\sim 130^\circ$. Interestingly, at MPC=512, the CO_2 was also found to form second layer coordinated where the corresponding $\theta = 90^\circ$. The observed data suggest us to conclude that the CO_2 lying in this layer behave as the first shell coordination numbers of CO_2 located in the first layer (where $\theta = \sim 35^\circ$ and $\sim 130^\circ$). Simultaneously, they are also proposed to coordinate weakly to fill the rest space around the MOF-5 corner as the second layer. For the MOF-5 linker, the result indicates free orientation of the CO_2 molecules. No preferential configuration was detected. The average coordination numbers of CO_2 at the corner and the linker sites are 2.9 and 3.1 molecules, respectively.

Acknowledgement

The Thailand Research Fund (TRF: RTA 4980006), Commission on Higher Education (CHE: Postdoctoral Fellowship) and the Deutsche Forschungsgemeinschaft (Schwerpunktprogramm SPP 1362), are gratefully thank for the financial support. The Computational Chemistry Unit Cell (CCUC) at Department of Chemistry, Faculty of Science, Chulalongkorn University and the Scientific Mathematics Advanced Research Tasks at Department of Mathematics, Faculty of Science, Khon Kaen University, are acknowledged for all computer resources and other facilities.

References

- (1) H Li, M Eddaoudi, M O'Keeffe OM Yaghi: *Nature*, 42(1999) 276.
- (2) NL Rosi, J Eckert, M Eddaoudi, DT Vodak, J Kim, M O'Keeffe, OM Yaghi: *Science* 300 (2003) 1127.
- (3) JLC Rowsell, AR Millward, KS Park, OM Yaghi: *J. Am. Chem. Soc.* 126 (2004) 5666.
- (4) JLC Rowsell, EC Spencer, J Eckert, JAK Howard, OM Yaghi: *Science* 309 (2005) 1350.
- (5) S Keskin DS Sholl: *Ind. Eng. Chem. Res* 48(2009) 914.
- (6) J Gascon , U Aktay, MD Hernandez-Alonso, GPM van Klink, F Kapteijn: *J. Cat.* 261(2009) 75.
- (7) JG Harris KH Yung: *J. Phys. Chem.* 99(1995) 12021.
- (8) JA. Greathouse MD Allendorf: *J. Phys. Chem. C* 112(2008) 5795.
- (9) B Smith T Forester: *J. Molec. Graphics* 14(1996) 136.

VITAE

NAME: Tanawut Ploymeerusmee

DATE AND PLACE OF BIRTH: 13 January 1983 in Bangkok, Thailand

ELEMENTARY SCHOOL:

1989-1995 Nakprasith School, Nakornpathom

SECONDARY SCHOOL:

1995-2001 Nakprasith School, Nakornpathom

UNIVERSITY EDUCATION:

2001-2005 B. Sc. in Chemistry, Department of Chemistry, Faculty of Science,
Chulalongkorn University, Bangkok

2006-2009 M. Sc. in Petrochemistry and Polymer Science, Faculty of Science,
Chulalongkorn University, Bangkok